7. S. D. Ling, C. R. Johnson, S. D. Frusher, K. R. Ridgway, *Proc. Natl. Acad. Sci. U.S.A.* **106**, 22341–22345 (2009).
8. T. Wernberg *et al.*, *Ecol. Lett.* **13**, 685–694 (2010).
9. N. A. J. Graham, S. Jennings, M. A. MacNeil, D. Mouillot, S. K. Wilson, *Nature* **518**, 94–97 (2015).
10. S. Bennett, T. Wernberg, E. S. Harvey, J. Santana-Garcon, B. J. Saunders, *Ecol. Lett.* **18**, 714–723 (2015).
11. E. S. Poloczanska *et al.*, *Nat. Clim. Change* **3**, 919–925 (2013).
12. T. Wernberg *et al.*, *Curr. Biol.* **21**, 1828–1832 (2011).
13. A. Vergés *et al.*, *Proc. Biol. Sci.* **281**, 20140846 (2014).
14. Materials and methods are available as supplementary materials on *Science* Online.
15. A. Hobday, G. Pecl, *Rev. Fish Biol. Fish.* **24**, 415–425 (2014).
16. M. T. Burrows *et al.*, *Science* **334**, 652–655 (2011).
17. T. Wernberg *et al.*, *Nat. Clim. Change* **3**, 78–82 (2013).
18. J. Zinke *et al.*, *Nat. Commun.* **5**, 3607 (2014).
19. J. Lough, A. Sen Gupta, A. J. Hobday, in *Report Card of Marine Climate Change for Australia: Detailed Scientific Assessment*, E. S. Poloczanska, A. J. Hobday, A. J. Richardson, Eds. (Hobart, Tasmania, 2012); www.oceanclimatechange.org.au.
20. S. Bennett, T. Wernberg, B. Arackal Joy, T. de Bettignies, A. H. Campbell, *Nat. Commun.* **6**, 10280 (2015).
21. D. P. Thomson, R. C. Babcock, M. A. Vanderklift, G. Symonds, J. R. Gunson, *Estuar. Coast. Shelf Sci.* **96**, 105–113 (2012).
22. M. Feng, D. Slawinski, L. E. Beckley, J. K. Keesing, *Mar. Freshw. Res.* **61**, 1259–1267 (2010).
23. M. A. Coleman *et al.*, *J. Ecol.* **99**, 1026–1032 (2011).
24. M. Feng, M. J. McPhaden, S.-P. Xie, J. Hafner, *Scientific Reports* **3**, 1277 (2013).
25. W. Cai *et al.*, *Nat. Clim. Change* **5**, 132–137 (2015).
26. B. D. Toohey, G. A. Kendrick, E. S. Harvey, *Oikos* **116**, 1618–1630 (2007).
27. P. K. Dayton, M. J. Tegner, *Science* **224**, 283–285 (1984).
28. E. A. Martinez, L. Cardenas, R. Pinto, *J. Phycol.* **39**, 504–508 (2003).
29. M. T. Burrows *et al.*, *Nature* **507**, 492–495 (2014).
30. S. Bennett *et al.*, *Mar. Freshw. Res.* **67**, 47–56 (2016).

ACKNOWLEDGMENTS

This work was funded by the Australian Research Council (T.W., G.A.K.), the Hermon Slade Foundation (T.W., S.B.), a U.K. Natural Environment Research Council Independent Research Fellowship (D.A.S.), the Australian Institute of Marine Science (T.W., M.D., B.R.), the Australian National University (C.J.F.), the Western Australian Museum (J.F.), the Department of Parks and Wildlife (T.H.H., S.W.), CSIRO Oceans and Atmosphere (R.C.B., F.D., M.A.V.), Fisheries Research and Development Corporation project no. 2008/013 (R.K.H., G.A.K.), The Marsden Fund of The Royal Society of New Zealand (M.S.T.), and the WA Strategic Research Fund for the Marine Environment (R.B., M.A.V., J.F.). T.W. and S.B. conceptualized and wrote the manuscript; T.W., S.B., R.B., T.dB., K.C., M.D., F.D., J.F., C.J.F., J.S.-G., R.K.H., E.S.H., T.H.H., G.K., B.R., B.J.S., D.K.S., M.T., C.T., F.T., M.A.V., and S.W. provided data; and T.W., S.B., R.K.H., J.S.-G., and D.A.S. performed analyses and modeling. All authors discussed the results and commented on the manuscript. The data are provided in the supplementary materials. Additional information can be obtained from T.W. All authors declare no conflicting interests.

SUPPLEMENTARY MATERIALS

www.sciencemag.org/content/353/6295/169/suppl/DC1
Materials and Methods
Figs. S1 to S3
Tables S1 to S6
References (*31*–*70*)

18 January 2016; accepted 31 May 2016
10.1126/science.aad8745

STRUCTURAL BIOLOGY

Structural basis for membrane anchoring of HIV-1 envelope spike

Jyoti Dev,[1,2]* Donghyun Park,[3]* Qingshan Fu,[1] Jia Chen,[3,4] Heather Jiwon Ha,[3,4] Fadi Ghantous,[5] Tobias Herrmann,[2] Weiting Chang,[3] Zhijun Liu,[6] Gary Frey,[3,4] Michael S. Seaman,[5] Bing Chen,[3,4]† James J. Chou[1,6]

HIV-1 envelope spike (Env) is a type I membrane protein that mediates viral entry. We used nuclear magnetic resonance to determine an atomic structure of the transmembrane (TM) domain of HIV-1 Env reconstituted in bicelles that mimic a lipid bilayer. The TM forms a well-ordered trimer that protects a conserved membrane-embedded arginine. An amino-terminal coiled-coil and a carboxyl-terminal hydrophilic core stabilize the trimer. Individual mutations of conserved residues did not disrupt the TM trimer and minimally affected membrane fusion and infectivity. Major changes in the hydrophilic core, however, altered the antibody sensitivity of Env. These results show how a TM domain anchors, stabilizes, and modulates a viral envelope spike and suggest that its influence on Env conformation is an important consideration for HIV-1 immunogen design.

HIV-1 envelope spike [Env; trimeric $(gp160)_3$, cleaved to $(gp120/gp41)_3$] fuses viral and host cell membranes to initiate infection (*1*). Binding of gp120 to receptor (CD4) and co-receptor (e.g., CCR5 or CXCR4) trigger large conformational changes, leading to a cascade of refolding events in gp41 and ultimately to membrane fusion (*2*–*4*). Mature Env spikes, $(gp120/gp41)_3$, are the sole antigens on the virion surface; they often induce strong antibody responses in infected individuals (*5*, *6*). A vast amount of structural information is available for the ectodomain of Env, a primary target of the host immune system, but much less for its transmembrane domain (TMD), membrane-proximal external region (MPER), and cytoplasmic tail (CT), in the context of lipid bilayer. The cryo-EM (electron microscopy) structure of a detergent-solubilized clade B JR-FL EnvΔCT construct without the CT has been described recently (*7*), but its MPER and TMD are disordered, probably because detergent micelles failed to mimic a membrane environment.

The HIV-1 TMD is more conserved than a typical membrane anchor (fig. S1). Previous studies showed that mutations and truncations in the TMD indeed affect membrane fusion and viral infectivity (*8*–*11*). Presence of a GxxxG motif, often implicated in oligomeric assembly of TM helices (*12*), suggests clustering of TMDs in membrane (fig. S1). The presence of a conserved, positively charged residue (usually arginine) near the middle of the TMD suggests functions other than just spanning a bilayer. TM helices of many cell surface receptors are not merely inert anchors but play essential roles in receptor assembly and signal transmission. For example, we have shown that CT truncation affects the antigenic surface of the ectodomain of HIV-1 Env on the opposite side of the membrane (*13*). Thus, understanding the physical coupling (conformation and/or dynamics) between the CT and the ectodomain mediated by the TMD may guide design of immunogens that mimic native, functional Env and induce broadly neutralizing antibodies (bnAbs).

To characterize the TMD structure by nuclear magnetic resonance (NMR), we used a fragment of gp41 (residues 677 to 716; HXB2 numbering, fig. S1), derived from a clade D HIV-1 isolate 92UG024.2 (*14*). This construct, $gp41^{HIV1D(677\text{-}716)}$, contains a short stretch of MPER (residues 677 to 683); the TM segment (residues 684 to 705), defined by hydrophobicity; and a fragment previously assigned to the CT domain [residues 706 to 716, containing a tyrosine-based sorting motif (*15*, *16*)]. The $gp41^{HIV1D(677\text{-}716)}$ protein was purified and reconstituted into bicelles (fig. S2, A and B) (*17*–*19*) with an expected lipid-bilayer diameter of ~44 Å (fig. S2C) (*20*, *21*), thereby incorporating the refolded $gp41^{HIV1D(677\text{-}716)}$ into a membrane-like environment. The bicelle-reconstituted $gp41^{HIV1D(677\text{-}716)}$ migrated on SDS–polyacrylamide gel electrophoresis (SDS-PAGE) with a size close to that of a trimer (theoretical molecular mass 14.1 kDa) (fig. S2D), suggesting that the protein was trimeric and resistant to SDS denaturation. The reconstituted $gp41^{HIV1D(677\text{-}716)}$ protein in bicelles generated an NMR spectrum with excellent chemical-shift dispersion (fig. S3A). The equivalent protein constructs from isolates 92BR025.9 (clade C) and 92RU131.16 (clade G) gave similar NMR spectra (fig. S3, B and C), suggesting that the TMDs of most HIV-1 Envs have similar structures when reconstituted in bicelles. We completed the NMR structure of $gp41^{HIV1D(677\text{-}716)}$ using a previously described protocol (figs. S4 and S5) (*22*, *23*). The final ensemble of structures converged to a root mean

[1]Department of Biological Chemistry and Molecular Pharmacology, Harvard Medical School, 250 Longwood Avenue, Boston, MA 02115, USA. [2]Virology Program, Harvard Medical School, 260 Longwood Avenue, Boston, MA 02115, USA. [3]Division of Molecular Medicine, Boston Children's Hospital, 3 Blackfan Street, Boston, MA 02115, USA. [4]Department of Pediatrics, Harvard Medical School, 300 Longwood Avenue, Boston, MA 02115, USA. [5]Center for Virology and Vaccine Research, Beth Israel Deaconess Medical Center, 330 Brookline Avenue, Boston, MA 02215, USA. [6]State Key Laboratory of Molecular Biology, National Center for Protein Science Shanghai, Shanghai Institute of Biochemistry and Cell Biology, Chinese Academy of Sciences, Shanghai 200031, China.
*These authors contributed equally to this work. †Corresponding author. Email: bchen@crystal.harvard.edu

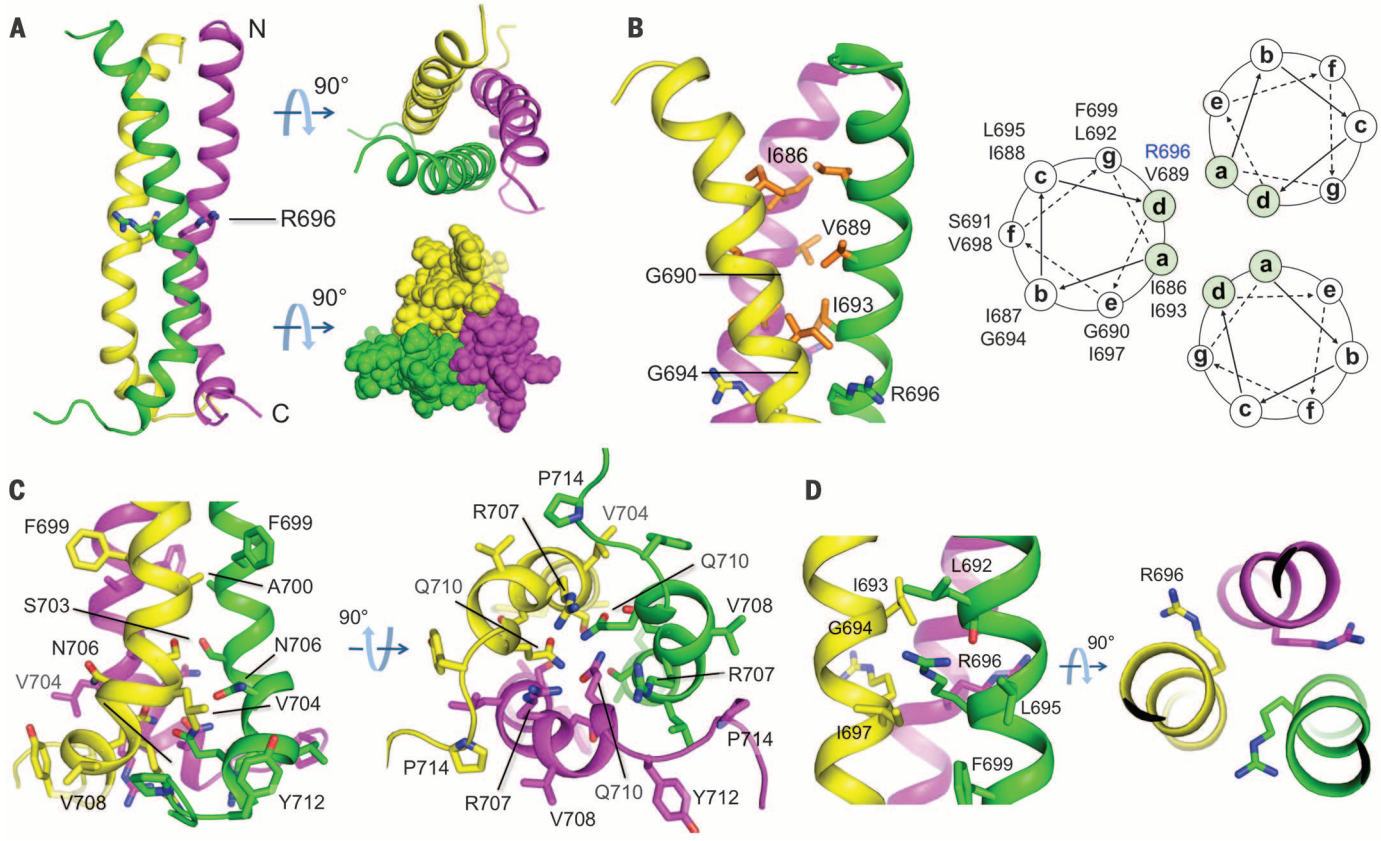

Fig. 1. NMR structure of the gp41$^{HIV1D(677-716)}$ trimer in bicelles. (**A**) Ribbon representation of the lowest-energy structure from the calculated ensemble. The sphere representation of the top view (lower right) shows that the trimer has no ion-permeable holes. (**B**) The N-terminal half of the structure with hydrophobic residues (orange) arranged in the coiled-coil pattern (right panel). (**C**) The C-terminal half of the structure showing an array of polar residues that form the C-terminal hydrophilic core. The network of polar contacts is hypothesized to stabilize the trimer. (**D**) Enlarged middle region of the structure showing the intramembrane R696 and its surrounding hydrophobic residues, as well as the backbone oxygen of L692. Single-letter abbreviations for the amino acid residues are as follows: A, Ala; C, Cys; D, Asp; E, Glu; F, Phe; G, Gly; H, His; I, Ile; K, Lys; L, Leu; M, Met; N, Asn; P, Pro; Q, Gln; R, Arg; S, Ser; T, Thr; V, Val; W, Trp; and Y, Tyr.

square deviation of 0.95 and 1.44 Å for backbone and all heavy atoms, respectively (fig. S6 and table S1).

gp41$^{HIV1D(677-716)}$ is a tightly assembled trimer ~54 Å long, with the conserved arginine (R696) near its midpoint (Fig. 1A). It shows a packing arrangement not seen in any other known TM helix dimers or trimers: Its N- and C-terminal halves have different modes of assembly, with an intervening kink. The N-terminal region is a conventional three-chain coiled-coil formed by residues 686 to 696 (Fig. 1B), including the GxxxG motif. The C-terminal half does not show classic "knobs-into-holes" interactions, but instead is held together by a network of polar contacts, mainly involving R707 and Q710, at the trimer interface of the kinked helical segments (residues 704 to 712) (Fig. 1C). We call this interface the "hydrophilic core."

R696, near the middle of each TM helix (Fig. 1D), produces three unbalanced charges at the center of the membrane. This residue occupies a "d" position in the heptad sequence (Fig. 1B). Its C^{β} points toward the threefold axis of the trimer, while the rest of the side chain bends away from the axis, placing the guanidinium group in a peripheral hydrophobic pocket formed by L692, L695, and I697 (Fig. 1D). The backbone carbonyl of L692 may form a hydrogen bond with one of the guanidinium NH_2 group of R696. H^{ε} of R696 showed a water nuclear Overhauser effect (NOE) in a ^{15}N-edited NOE spectrum (fig. S4), indicating the presence of an adjacent structured water. Thus, the guanidinium group, presumably charged at pH 6.7 under the NMR conditions, is partially neutralized by hydrogen bonding with the electronegative backbone oxygen of L692 and the water molecule. The polarizability of the hydrophobic pocket that surrounds the guanidinium may also lower its pK_a (acid dissociation constant) from its value in aqueous solution. Although well accommodated in the TMD trimer, the intramembrane R696 may modulate the stability of the helical trimer if the helices dissociate at any stage in assembly or fusion. The ^{1}H-^{15}N correlation spectrum of the gp41$^{HIV1D(677-716)}$ trimer showed inhomogeneous peak linewidth, with the N-terminal half near R696 having the most severe peak broadening, consistent with conformational fluctuation (fig. S7).

To confirm membrane partition of the TMD trimer, we used a paramagnetic probe, Gd(DOTA) (*24*), to measure solvent exposure of the four arginine residues in the gp41$^{HIV1D(677-716)}$ trimer. These arginines are distributed at different positions along the TM helices and thus serve as four depth markers. We measured intensity decrease of the arginine Hε-Nε correlation peaks at increasing concentrations of Gd(DOTA). The most solvent-exposed R707 showed the highest sensitivity to Gd(DOTA), whereas the most buried R696 was the least sensitive (Fig. 2A). R683 and R709 are near opposite lipid headgroup regions in the structure. R709 showed a greater resonance broadening than did R683, indicating that the latter is more deeply buried. We placed the gp41$^{HIV1D(677-716)}$ trimer in the lipid bilayer so that the four arginine positions were consistent with their respective sensitivity to Gd(DOTA) (Fig. 2B). This placement, which is consistent with the surface distribution of hydrophobic, polar, and charged residues (Fig. 2C), places R696 in a fully hydrophobic environment, slightly closer to the cytoplasmic side of the membrane. The MPER segment is in the headgroup region of the outer leaflet. The C-terminal segment, previously assigned to the CT, is at the headgroup-water interface of the inner leaflet.

To assess the contribution of specific residues to TMD stability, we generated 12 gp41$^{HIV1D(677-716)}$ mutants with single or double mutations, mainly

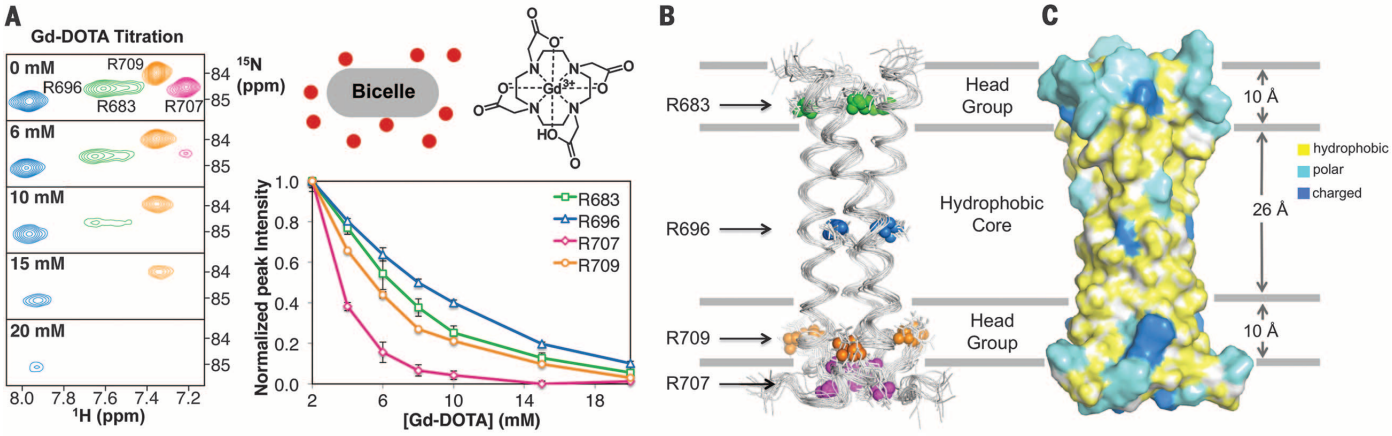

Fig. 2. Partition of the gp41$^{HIV1D(677-716)}$ trimer in lipid bilayer. (**A**) Measurement of membrane immersion depth of the four arginines using the water-soluble and membrane-inaccessible paramagnetic probe Gd-DOTA. The ^{1}H-^{15}N correlation peaks of the arginine Hε-Nε recorded in q = 0.5 bicelles (left) showed reduced peak intensity with increasing Gd-DOTA concentration (right) due to paramagnetic relaxation enhancement (PRE). R683 is shown in green, R696 in blue, R707 in magenta, and R709 in orange. Error bars represent spectra noise level normalized against maximum reference peak intensity. (**B**) Placement of the trimer structure in the presumed DMPC lipid bilayer, which is slightly thinner than the characterized thickness of DOPC bilayer (*35*), such that the positions of the four arginines are in accordance with the PRE results in (A). The positions of the arginine side chains are indicated by the Hε (spheres) in the ensemble of 15 low-energy structures. The color scheme is the same as in (A). (**C**) Surface representation of the lowest-energy structure positioned in DMPC bilayer as in (B) for showing the surface distribution of hydrophobic, polar, and charged amino acids. The hydrophobic residues (yellow) include A, I, L, F, V, P, and G; the polar residues (cyan) include Q, N, H, S, T, Y, C, M, and W; the charged residues (blue) include K, R, D, and E.

in the trimer interface. To introduce large-scale changes in the hydrophilic core, we also created mutants Δ(705–716) and G690L/Δ(705–716) with residues 705 to 716 deleted, and mutants 704–713 and G690L/704–713 with residues 704 to 713 mutated (Fig. 3 and table S2). We analyzed these mutants by SDS-PAGE after reconstitution in bicelles (fig. S8). Most simple mutations, including I686A, I693A, and R696N, did not disrupt the trimer completely, but only shifted the band to molecular mass positions lower than that of the wild type, indicating only partial trimer destabilization (fig. S8). We observed a similar pattern for mutants 704–713, G690L/704–713, and Δ705–716. The only mutant that migrated as a monomer was G690L/Δ705–716, with the GxxxG motif mutated and the entire hydrophilic-core region truncated (fig. S8). Thus, both the coiled-coil and the hydrophilic core contribute to the extraordinary stability of the TMD, and either one of them is sufficient to prevent the trimer from complete dissociation in bicelles.

To elucidate functional roles of the structural elements in the TMD, we mutated each of them in the intact Env spike and analyzed the effect on Env biogenesis, membrane fusion, and viral infectivity. We generated 27 Env mutants, using the sequence of a clade A isolate 92UG037.8, with single, double, or triple mutations in the coiled-coil region, R696 and its protecting residues, the kink, the hydrophilic core, or combinations of these elements (table S2). We also produced mutants 704–713 and G690L/704–713. When transiently transfected in 293T cells, all mutants expressed comparable levels of Env, with similar extents of cleavage between gp120 and gp41, as well as similar cell-surface levels (figs. S9 and S10). At a high Env expression level, at which cell-cell fusion was resistant to most neutralizing antibodies, the fusion activity of the TMD mutants was indistinguishable (93 to 109%) from that of the wild type (fig. S11). When the expression level was reduced to mimic the low surface density on HIV-1 virions (*25*), several TMD mutants, including R696A, had significantly lower cell-cell fusion activity than did the wild type (table S2 and fig. S12). Likewise, when these mutations were introduced into pseudoviruses, there were no major differences in Env incorporation and processing, but limited changes in infectivity for most of them (table S2 and figs. S13 and S14). R696A had almost full wild-type infectivity, whereas 704–713 and G690L/704–713 had substantially less—just the opposite of their effects on cell-cell fusion (table S2 and fig. S14).

To determine whether mutations in the TMD can influence the antigenic structure of the Env ectodomain and whether they might affect its antibody sensitivity, we used the cell-cell fusion assay to test inhibition of each Env mutant by a trimer-specific bnAb PG16 and by a nonneutralizing V3 antibody 3791 (table S3). Most mutants were essentially identical to the wild type in their sensitivity to either antibody; mutants I686A, Y712A, P714N, G690L/Y712A, G690L/P714N, G690L/P714K, and G690L/P714H exhibited detectable differences (fig. S15). We observed the most pronounced differences for mutants 704–713 and G690L/704–713, for which PG16 and 3791 switched phenotypes—the former became inactive and the latter inhibitory (fig. S15). All mutations that affect antibody inhibition are located in either the coiled-coil or the hydrophilic core. We infer that changes in TMD stability influence the antigenic structure of the ectodomain of the functional Env. When tested in a pseudovirus-based neutralization assay with bnAbs PG9 (trimer specific), 3BNC117 (CD4 binding site), 10-1074 (glycan- and V3-dependent), 10E8 (MPER), and 3791 (table S3), most mutants, except for 704–713 and G690/704–713, were unchanged in their sensitivity to PG9, 3BNC117, 10-1074 and 3791, but most became more sensitive to 10E8 (table S4). This result suggests that the changes produced by all the mutations tested, except for 704–713 and G690/704–713, are limited to local structure. In contrast, the mutants 704–713 and G690/704–713 became resistant to PG9 and sensitive to 3791—reflecting their properties in the cell-cell fusion assay. Mutant 704–713 was analyzed with additional antibodies. For cell-cell fusion, wild-type Env is sensitive to trimer-specific bnAbs PG9, PG16, and PGT145 and resistant to nonneutralizing antibodies b6 (CD4 binding site), 3791, and 17b (CD4-induced) (table S3, Fig. 3A, and fig. S16). The antibody inhibition pattern is reversed, however, for the fully functional mutant 704–713, indicating that the hydrophilic core of the TMD plays an important role in stabilizing and modulating the antigenic structure of the Env spike. Similar phenotypes were also observed with a 704–713 mutant derived from a clade C strain C97ZA012 (fig. S17). The pseudovirus neutralization assay gave similar, but less pronounced, results for the mutant 704–713 (Fig. 3B and table S4).

The most important finding from this study relevant to vaccine development is how the TMD modulates the antigenic surfaces of the Env spike. We reported previously that truncation of the CT domain of HIV-1 Env reshapes the antigenic surfaces of its ectodomain (*13*). We now show that mutations destabilizing the hydrophilic core of the TMD trimer resemble the CT deletion in altering the sensitivity of the functional Env to both nonneutralizing and trimer-specific neutralizing antibodies. In particular, the trimer-specific bnAbs, which neutralize by stabilizing the native

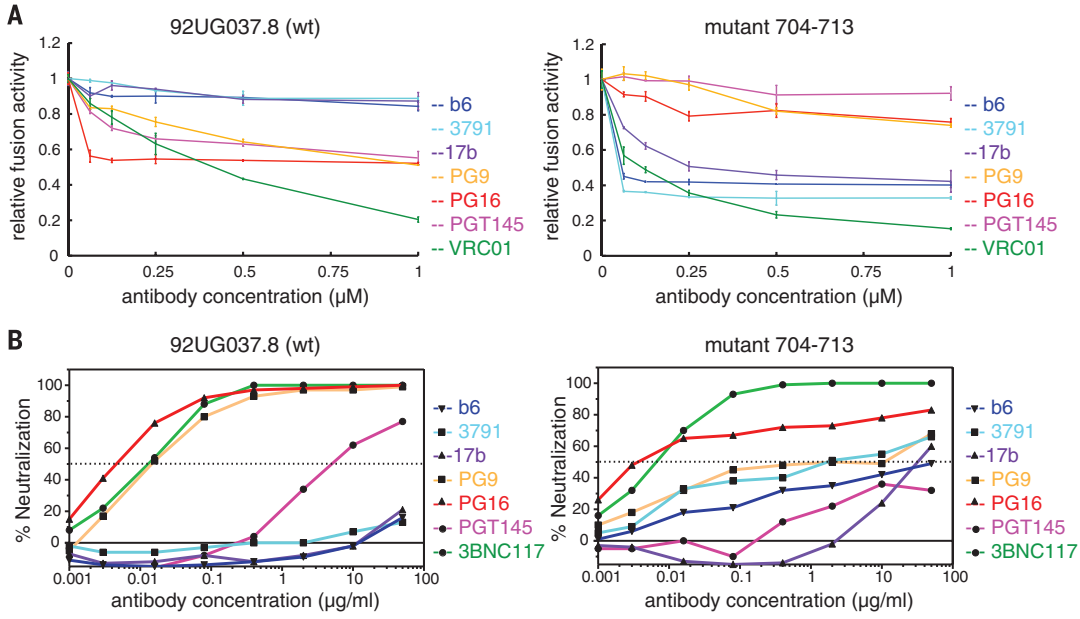

Fig. 3. Effect of mutations in the TMD of HIV-1 Env on its antibody sensitivity. (**A**) Antibody inhibition of cell-cell fusion mediated by the wild-type 92UG037.8 Env (left) and the TMD mutant 704–713 [right; residues 704 to 713 (VINRVRQGYS) were mutated to SSAASAAGSA] was analyzed with both nonneutralizing antibodies—including b6 (CD4 binding site; blue), 3791 (V3; cyan), and 17b (CD4-induced; purple)—and trimer-specific bnAbs, including PG9 (orange), PG16 (red), and PGT145 (magenta). The CD4 binding site bnAb VRC01 (green) was a control antibody. The experiment was carried out in triplicate and repeated at least twice with similar results. Error bars indicate the SD calculated by the Excel STDEV function. (**B**) Antibody neutralization of pseudoviruses containing either the 92UG037.8 Env (left) or the TMD mutant 704–713 (right) was determined with antibodies b6, 3791, 17b, PG9, PG16, and PGT145, shown in the same color scheme as in (A). The CD4 binding site bnAb 3BNC117 was a control antibody (green). The experiment was performed in duplicate.

conformation of Env (*26*, *27*), do not recognize the Env spike when its TMD has been destabilized. We suggest that the TMD mediates conformational coupling between the ectodomain and the CT and that the trimeric structure seen by NMR represents the conformation of the TMD adopted by a native Env spike in a membrane.

The placement of gp41$^{HIV1D(677-716)}$ in a lipid bilayer reveals clear boundaries of the TM segment and settles a contentious issue (*10*, *28*). Part of the 10E8 epitope (residues 677 to 683) is embedded in the headgroup layer of the outer leaflet, consistent with lack of accessibility of this epitope on the native Env (*13*, *29*). The hydrophilic core, which was thought to be part of the CT, is similarly protected by the headgroup layer of the inner leaflet. This hydrophilic region contains a tyrosine-based sorting signal (^{712}YSPL^{715}), which may participate in Env internalization by endocytosis (*15*, *16*, *30*). Our structure indicates that Y712 and P714 in this motif on one TM protomer interact with L704 and V708 of the adjacent protomer, respectively, thereby also contributing to trimer stability.

The TMD is required not only for membrane anchoring and fusion, but also for stability of the entire Env spike. This observation can explain why most soluble Env preparations with the TMD deleted, except for those of a few selected strains (*31*, *32*), are unstable and conformationally heterogeneous, unless they have specific, stabilizing modifications (*26*, *33*, *34*). To design immunogens that mimic optimally native viral spikes, one must not ignore structural constraints imposed by the TMD on the ectodomain. The high-resolution structure of the HIV-1 Env TMD trimer presented here can be a guide for engineering more effective immunogens.

REFERENCES AND NOTES

1. S. C. Harrison, *Nat. Struct. Mol. Biol.* **15**, 690–698 (2008).
2. D. C. Chan, D. Fass, J. M. Berger, P. S. Kim, *Cell* **89**, 263–273 (1997).
3. W. Weissenhorn, A. Dessen, S. C. Harrison, J. J. Skehel, D. C. Wiley, *Nature* **387**, 426–430 (1997).
4. M. Pancera *et al.*, *Nature* **514**, 455–461 (2014).
5. X. Wei *et al.*, *Nature* **422**, 307–312 (2003).
6. D. D. Richman, T. Wrin, S. J. Little, C. J. Petropoulos, *Proc. Natl. Acad. Sci. U.S.A.* **100**, 4144–4149 (2003).
7. J. H. Lee, G. Ozorowski, A. B. Ward, *Science* **351**, 1043–1048 (2016).
8. R. J. Owens, C. Burke, J. K. Rose, *J. Virol.* **68**, 570–574 (1994).
9. L. Shang, L. Yue, E. Hunter, *J. Virol.* **82**, 5417–5428 (2008).
10. L. Yue, L. Shang, E. Hunter, *J. Virol.* **83**, 11588–11598 (2009).
11. E. Helseth *et al.*, *J. Virol.* **64**, 6314–6318 (1990).
12. M. G. Teese, D. Langosch, *Biochemistry* **54**, 5125–5135 (2015).
13. J. Chen *et al.*, *Science* **349**, 191–195 (2015).
14. F. Gao *et al.*, *J. Virol.* **70**, 1651–1667 (1996).
15. J. F. Rowell, P. E. Stanhope, R. F. Siliciano, *J. Immunol.* **155**, 473–488 (1995).
16. M. Boge, S. Wyss, J. S. Bonifacino, M. Thali, *J. Biol. Chem.* **273**, 15773–15778 (1998).
17. M. E. Call *et al.*, *Cell* **127**, 355–368 (2006).
18. M. E. Call, K. W. Wucherpfennig, J. J. Chou, *Nat. Immunol.* **11**, 1023–1029 (2010).
19. To produce the protein, we expressed the His-tagged TrpLE-gp41$^{HIV1D(677-716)}$ fusion protein in *Escherichia coli* as inclusion bodies, purified the solubilized protein by Ni-affinity chromatography, removed the TrpLE tag with cyanogen bromide, and separated the product by reverse-phase high-performance liquid chromatography. Bicelles were made of 1,2-dimyristoyl-sn-glycero-3-phosphocholine (DMPC; lipid) and 1,2-dihexanoyl-sn-glycero-3-phosphocholine (DHPC; detergent) at a ratio (*q*) of 0.5. In this report, we use gp41$^{HIV1D(677-716)}$ and TMD interchangeably for convenience.
20. K. J. Glover *et al.*, *Biophys. J.* **81**, 2163–2171 (2001).
21. C. R. Sanders 2nd, J. P. Schwonek, *Biochemistry* **31**, 8898–8905 (1992).
22. B. OuYang *et al.*, *Nature* **498**, 521–525 (2013).
23. For structure determination, we proceeded with the clade D construct because its expression level was the highest. The approach involves determination of local structures of the monomers and assembly of the trimer with intermonomer distance restraints derived from NOEs between structurally equivalent but isotopically differently labeled subunits. We could identify eight intermonomer NOEs using the isotopically mixed labeled sample to calculate a unique assembly solution, which was further validated and refined with other conventional NOE data.
24. Gd(DOTA) is a water-soluble and membrane-inaccessible molecule, so that the paramagnetic relaxation enhancement (PRE) it generates decreases with distance from the bilayer surface.
25. P. Zhu *et al.*, *Nature* **441**, 847–852 (2006).
26. R. W. Sanders *et al.*, *PLOS Pathog.* **9**, e1003618 (2013).
27. J. P. Julien *et al.*, *Proc. Natl. Acad. Sci. U.S.A.* **110**, 4351–4356 (2013).
28. J. T. West, P. B. Johnston, S. R. Dubay, E. Hunter, *J. Virol.* **75**, 9601–9612 (2001).
29. J. Chen *et al.*, *J. Virol.* **88**, 1249–1258 (2014).
30. C. Berlioz-Torrent *et al.*, *J. Virol.* **73**, 1350–1361 (1999).
31. S. A. Jeffs *et al.*, *Vaccine* **22**, 1032–1046 (2004).
32. J. M. Kovacs *et al.*, *Proc. Natl. Acad. Sci. U.S.A.* **111**, 18542–18547 (2014).
33. J. Guenaga *et al.*, *J. Virol.* **90**, 2806–2817 (2015).
34. Y. Do Kwon *et al.*, *Nat. Struct. Mol. Biol.* **22**, 522–531 (2015).
35. M. C. Wiener, S. H. White, *Biophys. J.* **61**, 434–447 (1992).

ACKNOWLEDGMENTS

We thank S. Harrison and S. Rits-Volloch for generous advice and assistance; D. Barouch, B. Haynes, and A. Carfi for critical reading of the manuscript; and the NIH AIDS Reagent Program, Division of AIDS, National Institute of Allergy and Infectious Diseases, NIH, for reagents. The data presented in this manuscript are tabulated in the main paper and in the supplementary materials. The atomic structure coordinate and structural constraints are deposited in the Protein Data Bank under the accession number 5JYN. The chemical-shift values are deposited in the Biological Magnetic Resonance Data Bank under the accession number 30090. This work was supported by NIH grants AI084794 (to B.C. and Dan H. Barouch), GM083680 (to B.C.), AI106488 (to B.C.), HL103526 (to J.J.C.), and AI127193 (to B.C. and J.J.C.), Collaboration for AIDS Vaccine Discovery (CAVD) grant OPP1040741 (to Dan H. Barouch from the Bill and Melinda Gates Foundation), and the Center for HIV/AIDS Vaccine Immunology–Immunogen Design AI-100645 (to Barton F. Haynes). The NMR data were collected at the NMR facility of National Center for Protein Science Shanghai (supported by Chinese Academy of Sciences grant XDB08030301) and Massachusetts Institute of Technology–Harvard Center for Magnetic Resonance (supported by NIH grant P41 EB-002026).

SUPPLEMENTARY MATERIALS

www.sciencemag.org/content/353/6295/172/suppl/DC1
Materials and Methods
Figs. S1 to S20
Tables S1 to S4
References (*36*–*52*)

17 March 2016; accepted 13 June 2016
Published online 23 June 2016
10.1126/science.aaf7066

Structural basis for membrane anchoring of HIV-1 envelope spike

Jyoti Dev, Donghyun Park, Qingshan Fu, Jia Chen, Heather Jiwon Ha, Fadi Ghantous, Tobias Herrmann, Weiting Chang, Zhijun Liu, Gary Frey, Michael S. Seaman, Bing Chen, and James J. Chou

Science, **353** (6295), .
DOI: 10.1126/science.aaf7066

Env's transmembrane domain revealed

HIV-1's envelope protein (Env) spans the viral membrane and grants the virus entry into host cells. Env is also the sole protein of HIV-1 that is targeted by antibodies, making it a key target for vaccine design. Dev *et al.* used nuclear magnetic resonance to determine an atomic-level structure of the membrane-spanning region of Env in a lipid bicelle. Env's transmembrane domain forms a well-ordered trimer, which includes a stabilizing C-terminal hydrophilic core. Disrupting this core alters the sensitivity of Env to broadly neutralizing antibodies, suggesting the potential importance of this region to vaccine design.

Science, this issue p. 172

Supplementary Materials for

Structural basis for membrane anchoring of HIV-1 envelope spike

Jyoti Dev, Donghyun Park, Qingshan Fu, Jia Chen, Heather Jiwon Ha, Fadi Ghantous, Tobias Herrmann, Weiting Chang, Zhijun Liu, Gary Frey, Michael S. Seaman, Bing Chen,* James J. Chou

*Corresponding author. Email: bchen@crystal.harvard.edu

Published 23 June 2016 on *Science* First Release
DOI: 10.1126/science.aaf7066

This PDF file includes:

Materials and Methods

Protein expression and purification

HIV-1 gp41(677-716) fragments from the clade C isolate 92BR025.9 (with M687K mutation), the clade D 92UG024.2 (designated $gp41^{HIV1D(677-716)}$) and the clade G 92RU131.16 were synthesized by GenScript (Piscataway, NJ). Expression constructs were created by fusing the gp41(677-716) fragments to the C-terminus of the His9-TrpLE expression sequence in pMM-LR6 vector (a gift from S.C. Blacklow, Harvard Medical School), with an added methionine in-between for cleavage by cyanogen bromide. Constructs with mutations in the TMD were generated by standard PCR protocols and confirmed by DNA sequencing. For NMR sample preparation, transformed *E. coli* strain BL21 (DE3) cells were grown in 1L M9 minimal media supplemented with Centrum multivitamins and stable isotopes. Cultures were grown at 37°C to an absorbance of ~0.7 at 600 nm, and cooled to 18°C before induction with 500 μM isopropyl β-D-thiogalatopyranoside at 18°C for overnight. For fully deuterated proteins, bacterial cultures were grown in D_2O (Sigma Aldrich, St. Louis, MO) with deuterated glucose (Cambridge Isotope Laboratories, Tewksbury, MA).

Cells were harvested after overnight growth, suspended in a lysis buffer (50 mM Tris, pH 8.0 and 200 mM NaCl), and lysed by sonication. Inclusion bodies were separated by centrifugation at 8,000 xg and suspended in a denaturing buffer (1% Triton X-100, 6 M guanidine hydrochloride, 50 mM Tris, pH 8.0 and 200 mM NaCl). The fusion protein was bound to nickel affinity resin (Sigma Aldrich), washed with a washing buffer (8M Urea, 50 mM Tris, pH 8.0 and 200 mM NaCl) and deionized H_2O, and finally eluted with 90% formic acid. The HIV-1 gp41(677-716) protein was released from the 14-kilodalton TrpLE by cleavage at the methionine using cyanogen bromide (0.1g/ml) in 90% formic acid for 1 hr. The cleavage reaction mixture was then dialyzed to remove excess cyanogen bromide and lyophilized. Proteins were dissolved in 90% formic acid and separated by reverse-phase high performance liquid chromatography (RP-HPLC) in a Zorbax SB-C3 column (Agilent Technologies, Santa Clara, CA) with a gradient from 5% isopropanol (0.1% trifluoroacetic acid) to 75% isopropanol and 25% acetonitrile (0.1%

trifluoroacetic acid). Fractions containing the HIV-1 gp41(677-716) protein were collected, lyophilized. Protein identity was confirmed by MALDI-TOF mass spectrometry and SDS-PAGE.

Reconstitution of HIV-1 gp41(677-716) in bicelles

To reconstitute in bicelles, 1-2 mg of lyophilized HIV-1 gp41(677-716) protein was mixed with 12 mg 1,2-Dimyristoyl-*sn*-Glycero-3-Phosphocholine (DMPC; protonated from Avanti Ploar Lipids, Alabaster, AL or deuterated from FB Reagents, Boston, MA) and ~30 mg 1,2-Dihexanoyl-*sn*-Glycero-3-Phosphocholine (DHPC; protonated from Avanti Ploar Lipids or deuterated from FB Reagents). The mixture was then dissolved in 3 ml of 8 M Urea, and dialyzed twice against 25 mM MES buffer (pH 6.7) to remove the denaturant. Since some DHPC was lost during dialysis, it was added back after dialysis to make the final DMPC: DHPC ratio ~1:2. The DMPC:DHPC ratio was monitored by 1D NMR throughout the reconstitution process and verified in the final NMR sample. The sample was concentrated using Centricon (EMD Millipore, Billerica, MA) to ~300 μl. The final NMR sample contains ~0.8 mM monomeric HIV-1 gp41(677-716) protein, 60 mM DMPC, 120 mM DHPC, 25 mM MES (pH 6.7), 0.1% NaN_3 and 6% D_2O. For NOESY experiments, the protein was reconstituted in DMPC and DHPC with deuterated acyl chains.

NMR spectroscopy

All NMR data was collected at 30°C on Bruker spectrometers operating at ^{1}H frequency of 900 MHz, 750 MHz, or 600 MHz and equipped with cryogenic probes. NMR data was processed using NMRPipe (*36*) and spectra analysis was performed in NMRPipe, CCPNMR (*37*) and XEASY (*38*).

Sequence-specific assignments of backbone amide resonance were determined from two pairs of gradient-selected, TROSY-enhanced triple resonance experiments (*39*), collected on a uniformly (^{15}N, ^{13}C, ^{2}H)-labeled sample using 750 MHz spectrometer. The triple resonance experiments included HNCA, HN(CO)CA, HN(CA)CO and HNCO. Backbone amide resonance assignments were confirmed in a ^{15}N-edited NOESY-TROSY-HSQC

spectrum with 100ms NOE mixing time (τ_{NOE}), which was recorded on a 900 MHz spectrometer on uniformly (^{15}N, ^{13}C)-labeled sample. The ^{15}N-edited NOESY-TROSY-HSQC (τ_{NOE}= 100ms) and ^{13}C-edited NOESY-HSQC (τ_{NOE}= 150ms) were used to assign protein aliphatic and aromatic side chain resonances. Stereospecific assignments of methyl groups were determined from a constant-time (28 ms) ^{1}H-^{13}C HSQC spectrum recorded on a 15% ^{13}C-labeled sample.

Intramolecular distance restraints derived from nuclear Overhauser enhancements (NOEs) were obtained from the above mentioned ^{15}N-edited and ^{13}C-edited NOESY experiments. A combination of intramolecular distance restrains and backbone dihedral angles, obtained from chemical shifts, were used to define the helical region of the monomer. Determining the intermolecular distance restraints faced the challenge of measuring NOEs between structurally equivalent subunits having the same chemical shifts. To solve this problem, we prepared mixed sample in which half of the monomers were ^{15}N, ^{2}H-labeled and the other half 15% ^{13}C-labeled. Recording a 3D ^{15}N-edited NOESY-TROSY-HSQC (τ_{NOE} = 300 ms) on this sample allowed measurement of exclusive NOEs between the ^{15}N-attached protons of one subunit and aliphatic protons of the neighboring subunits. The non-deuterated peptide was 15% ^{13}C-labeled for recording the ^{1}H-^{13}C HSQC spectrum as internal aliphatic proton chemical shift reference. An additional ^{15}N-edited NOESY spectrum (τ_{NOE} = 60 ms) was recorded on a ^{15}N-labeled sample to assign Hε-Nε resonances of arginine and confirm presence of water NOE to arginine Hε-Nε.

Structure calculation

Structure was calculated using the program XPLOR-NIH (*40*). First, the monomer structure was derived using intramonomer restraints and backbone dihedral restraints, determined from chemical shifts using the TALOS+ program (*41*). The dihedral restraints and uncertainties from TALOS+ program were used as restraints in XPLOR calculation because the statistics for N, Cα and C' chemical shift derived ϕ and ψ were considered "good" by TALOS+ (except for G711 and L715, which were not used) (Fig. S18). In total, 10 monomer structures were calculated using a standard simulated annealing (SA)

protocol. We then used three copies of the lowest energy monomer structure to construct an initial model of the trimer using intermonomer distance restraints from the NOESY experiment collected on mixed samples. For each intermonomer restraint between two adjacent monomers, three identical distance restraints were assigned respectively to all pairs of neighboring monomers to satisfy the condition of C3 rotational symmetry. The assembled trimer was then refined against the complete set of NOE restraints (both intramonomer and intermonomer) and dihedral angles using a SA protocol in which the temperature in the bath was cooled from 1000K to 20K. The NOE restraints were enforced by flat-well harmonic potentials, with the force constant ramped from 25 to 50 kcal/mol $Å^{-2}$ during annealing. For the defined helical regions, backbone dihedral angle restraints (Φ = -60°, Ψ = -40°) were applied, all with a flat-well (±10°) harmonic potential with force constant ramped from 15 to 30 kcal/mol rad^{-2}. A total of 75 structures were calculated and 15 lowest energy structures were selected as the final structural ensemble. The assignment completeness for different nuclei are: N, 92.5%; H, 94.87%; CO, 97.50%; CA, 97.50%; HA, 95.35%; Methyl C, 97.30%; Methyl H, 97.30%; all other H - 71.95%. Additional data are also shown in Figs. S19 and S20.

Generation of Env mutant constructs and production of monoclonal antibodies

Full-length Env mutants were generated using the 92UG037.8 or C97ZA012 gp160, described previously (*13*), as a template by QuikChange Site-Directed Mutagenesis (Agilent Technologies). All constructs were confirmed by restriction digestion and DNA sequencing. Anti-HIV-1 Env monoclonal antibodies and their Fab fragments were produced as described (*13, 42*). We have generated expression constructs of antibodies PG9, PG16, PGT145 and 10E8 using synthetic genes made by GeneArt Gene Synthesis (Life Technologies, Carlsbad, CA) or GenScript. The VRC01 expression construct was kindly provided by John Mascola (VRC, NIH); antibodies 10-1074 and 3BNC117 by Michel Nussenzweig (Rockefeller University); the CHO stable line expressing antibody b6 by Dennis Burton (Scripps); 17b hybridoma by James Robinson (Tulane University); 3791 hybridoma by Susan Zolla-Pazner (New York University). The expression constructs of 10E8 were initially obtained from the NIH AIDS reagent program.

Production of pseudoviruses containing mutant Envs

Preparation of HIV-1 Env pseudoviruses containing mutations in the TMD, titration of pseudovirus stocks to determine the 50% tissue culture infectious dose per ml ($TCID_{50}$/ml) and dilution for use in neutralization assays were performed as previously described (*43*). Briefly, each pseudovirus was prepared by transfecting 293T/17 cells (ATCC, Manassas, VA) with 4 μg of Env expression plasmid and 8 μg of an Env-deficient HIV-1 backbone vector (pSG3ΔEnv). Pseudovirus-containing culture supernatant was harvested 24 hours after transfection, filtered (0.45 μm), and stored at −80°C. To determine $TCID_{50}$/ml, a 5-fold serial dilution of virus stock was performed in quadruplicate wells and incubated with TZM.bl cells (NIH AIDS reagent program) in growth media containing DEAE-dextran (Sigma-Aldrich) at a final concentration of 11 μg/ml. After 48 hours, the cells were measured for luciferase reporter gene expression, indicating the ability of the pseudovirus to infect cells. $TCID_{50}$/ml was calculated using an Excel macro made available on the Las Alamos National Laboratories website (www.hiv.lanl.gov).

HIV-1 p24 Antigen ELISA assay

Viral stocks were boiled in a buffer containing 0.5% Triton X-100 for 60 min and analyzed for p24 antigen using a HIV-1 p24 antigen ELISA 2.0 kit (ZeptoMetrix Corporation, Buffalo, New York). Briefly, virus samples were diluted with the assay diluent provided in the kit, loaded in duplicate onto a prewashed plate, and incubated at 37°C for 2 hr. The plate was then washed 6 times with 1X washing buffer, and incubated with an anti-p24 antibody conjugated with horseradish peroxidase for 1 hr. Substrate (tetramethylbenzidine) was then added to the wells, and incubated for 30 min at room temperature. Colorimetric reaction was terminated by addition of hydrochloric stop-solution (hydrochloric), and optical density (OD) was recorded at 450 nm using an Emax Precision Microplate Reader (Molecular Devices, LLC, Sunnyvale, CA).

Western blot

293T cells were transiently transfected with 5 μg of the 92UG037.8 gp160 expression construct or its TMD mutants. Lysates of cells expressing Env or its mutants were

prepared by resuspending the cells in PBS (phosphate buffered saline) at a density of $2x10^6$ cells/ml, followed by treatment with Laemmli Sample Buffer (Bio-Rad, Hercules, CA) and boiling for 10 min. Virus lysates were made by directly mixing p24-normalized virus stocks with Laemmli Sample Buffer and boiling for 10 min. Env samples were resolved in 4-15% Mini-Protean TGX gel (Bio-Rad) and transferred onto PVDF membranes (Millipore, Billerica, MA) by an Iblot2 (Life Technologies). Membranes were blocked with 5% skimmed milk in PBS for 1 hour and incubated with anti-V3 loop antibody 3791 for another hour at room temperature. Alkaline phosphatase conjugated anti-human Fab IgG (1:5000) (Sigma-Aldrich) was used as a secondary antibody. Env proteins were visualized using one-step NBT/BCIP substrates (Thermo Scientific, Cambridge, MA).

Flow cytometry

293T cells were transiently transfected with 2 μg of the 92UG037.8 gp160 expression construct or its TMD mutants in 6 wells plates. Env-expressing cells were detached from plates using PBS, and washed with ice-cold PBS containing 1% BSA. 10^6 cells were incubated for 30~40 minutes on ice with either VRC01 Fab, 2G12 Fab, or 10e8 IgG at concentrations of 10 μg/ml in PBS containing 1% BSA. The cells were then washed twice with PBS containing 1% BSA and stained with R-Phycoerythrin AffiniPure F(ab')2 fragment goat anti-human IgG, F(ab')2 Fragment specific secondary antibody (Jackson ImmunoResearch laboratories, West Grove, PA) at 5 μg/ml. All the fluorescently labeled cells were washed twice with PBS containing 1% BSA and analyzed immediately using a BD LSRII instrument and program FACSDIVA (BD Biosciences, San Jose, CA). All data were analyzed by FlowJo (FlowJo, LLC, Ashland, OR).

Cell-cell fusion assay and antibody inhibition

We have adapted an assay, based on the α-complementation of E. coli β-galactosidase, to analyze the Env-mediate cell-cell fusion (*44*). The function of an inactive mutant β-galactosidase with N-terminal residues 11-41 deleted (ω fragment) is rescued by its N-terminal fragment, called the α fragment, upon Env-mediated cell-cell fusion. 293T cells were cotransfected with either HIV-1 Env and the α fragment of β-galactosidase or CD4,

CCR5 and the ω fragment of β-galactosidase. Env-expressing cells ($2.0x10^6$ cells/ml) were mixed with CD4- and CCR5-expressing cells ($2.0x10^6$ cells/ml). Cell-cell fusion was allowed to proceed at 37°C for 2 hr. Cell-cell fusion activity was quantified using a chemiluminescent assay system, Gal-Screen (Applied Biosystems, Foster City, CA). Background signal was determined by carrying out the assay with cells lacking the Env gene. To analyze antibody inhibition, Env-expressing cells were first were incubated with antibodies at various concentrations (62.5 nM - 1 μM) at 37°C for 20 min before mixing with CD4- and CCR5-expressing cells. Antibodies used in this assay include Fab fragments of b6, 3791, 17b, PG9, PG16, PGT145 and VRC01.

Viral infectivity and antibody neutralization assays

Viral infectivity of HIV-1 92UG037.8 Env and its TMD mutants was measured by infecting TZM.bl cells with p24-normalized pseudovirus in growth media containing DEAE-dextran (11μg/ml). 48 hours post-infection, luciferase activity of the reporter gene was quantified as previously described (*45*). Likewise, neutralizing IC_{50} and IC_{80} titers of monoclonal antibodies were determined also by the luciferase-based virus neutralization assay in TZM.bl cells as previously described (*45*). The assay measures the reduction in luciferase reporter gene expression in TZM-bl cells following a single round of virus infection. Briefly, 5-fold serial dilutions of antibody samples were performed in duplicate (96-well flat bottom plate) in 10% DMEM growth medium (100 μl/well). Virus was added to each well in a volume of 50 μl, and the plates were incubated for 1 hour at 37°C. TZM.bl cells were then added (1×10^4/well in 100 μl volume) in 10% DMEM growth medium containing DEAE-Dextran. Following a 48 hour incubation, luminescence was measured using Bright-Glo luciferase reagent (Promega, Madison, WI). The IC_{50} and IC_{80} titers were calculated as the antibody dilution that resulted in a 50% or 80% reduction in relative luminescence units (RLU), respectively, compared with the virus control wells after the subtraction of cell control RLU. Maximum percent inhibition (MPI) indicates the highest percent inhibition of virus infection observed with the tested concentrations of each antibody. Murine leukemia virus (MuLV) was used as a negative control virus for all assays. Antibodies used in this assay include IgG of b6, 3791, 17b, PG9, PG16, PGT145 and 3BNC117.

Fig. S1

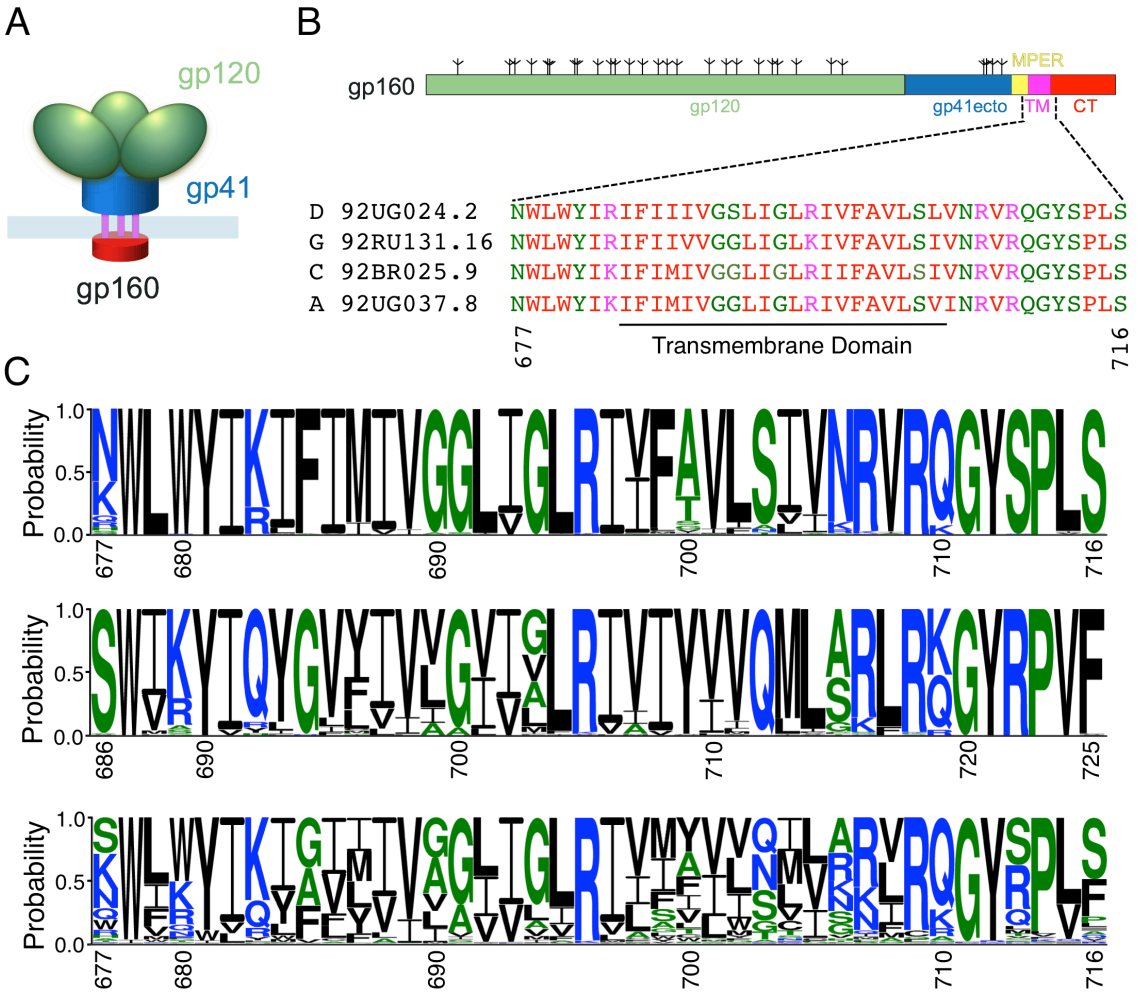

Figure S1. Schematic and sequence of the transmembrane segment of Env. (A) Schematic representation of HIV-1 Env trimer with gp120 in green, gp41 ectodomain in blue, the transmembrane domain (TMD) in magenta, and the cytoplasmic tail in red. **(B)** Location of the transmembrane segment in the gp160 schematic and sequence alignment of the HIV-1 gp41 fragment (residues 677-716; HXB2 numbering) from four selected isolates used in this study. The first three sequences were chosen because of their suitability for NMR studies and the 92UG037.8 sequence was used for functional studies. The 92BR025.9 construct contains M687K mutation, necessary for CNBr cleavage reaction during protein purification. The schematic is shown in the same color scheme as in (A) and the alignment is colored by ClustalW. **(C)** Sequence logos showing variations

in the gp41 segment (residues 677-716) among 5132 HIV-1 sequences (top), 113 HIV-2 sequences (middle) and 173 SIV sequences (bottom panel). They are colored according to their chemical properties: small amino acids are in green, hydrophobic amino acids in black, and strongly polar or charged basic residues in blue. The logos were generated using website tools of the Los Alamos National Laboratory, New Mexico, USA (http://www.hiv.lanl.gov/content/sequence/ANALYZEALIGN/analyze_align.html), as recommended by Dr. Bette Korber (Los Alamos National Laboratory).

Fig. S2

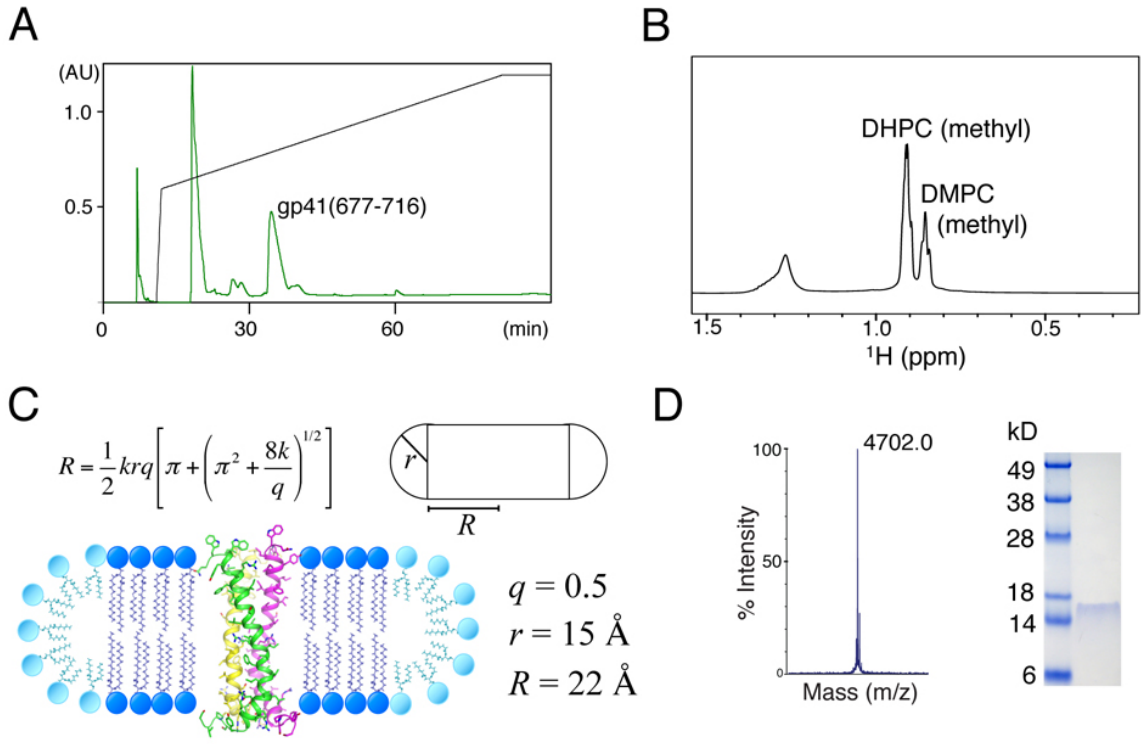

Figure S2. Purification and bicelle reconstitution of gp41$^{HIV1D\ (677\text{-}716)}$. (A) Reverse-phase HPLC purification of gp41$^{HIV1D\ (677\text{-}716)}$ after cleavage from the TrpLE fused protein. **(B)** The 1D ^{1}H NMR spectrum of a bicelle reconstituted gp41$^{HIV1D\ (677\text{-}716)}$ sample recorded at 600 MHz showing the molar ratio of DMPC to DHPC as ~ 0.5. **(C)** Illustration of gp41$^{HIV1D\ (677\text{-}716)}$ trimer in a DMPC (blue spheres)/DHPC (cyan spheres) bicelle. The radius of the bicelle is calculated using the displayed equation (*20*), in which, *R* and *r* are radiuses of planar and rim region, respectively; *q* is the molar ratio of DMPC to DHPC; and *k* is the ratio of headgroup areas for DHPC as compared with DMPC. The diameter (2*R*) of the planar region of a bicelle is calculated to be ~44 Å when $q = 0.5$. **(D)** MALDI-TOF mass spectrometry (left) of gp41$^{HIV1D\ (677\text{-}716)}$. The pure lyophilized protein was dissolved in isopropanol for mass spectrometry, giving an expected size of a monomer (theoretical M.W. of monomer is 4.7 kDa). SDS-PAGE (right) of bicelle-reconstituted gp41$^{HIV1D\ (677\text{-}716)}$. The protein migrates between the markers of 14 and 18 kDa and the calculated M.W. of trimer is ~14.1 kDa.

Fig. S3

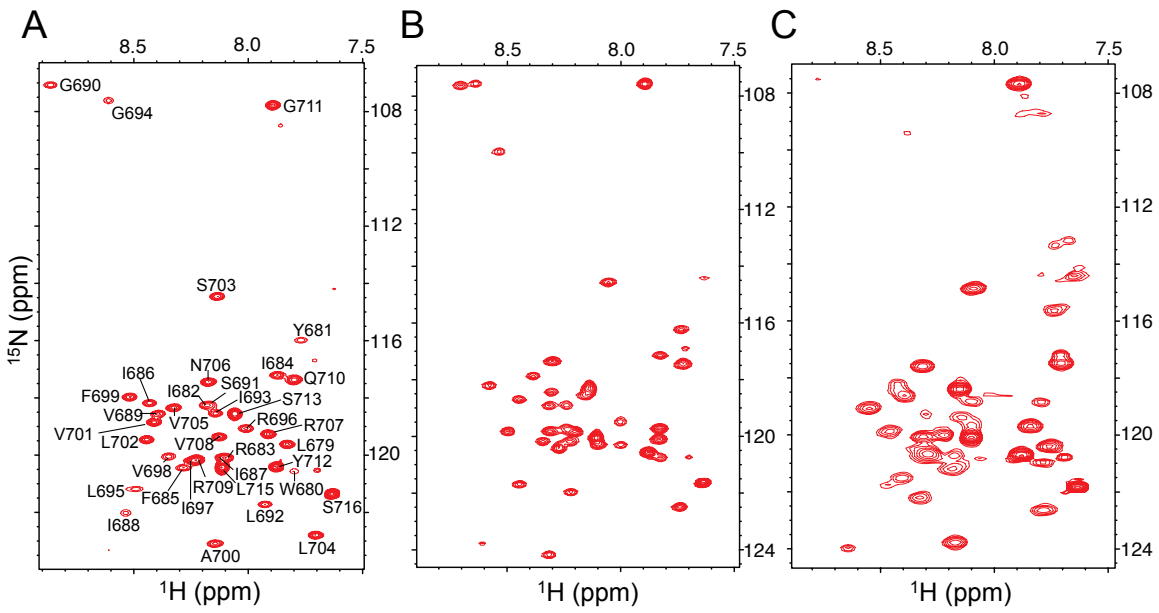

Figure S3. NMR spectra of gp41(677-716) derived from different HIV-1 isolates. Two-dimensional ^{1}H-^{15}N TROSY-HSQC spectra of bicelle-reconstituted gp41(677-716) samples: (^{2}H,^{15}N)-labeled sample from the HIV-1 clade D isolate 92UG024.2 (**A**), (^{2}H,^{15}N)-labeled sample from the clade G isolate 92RU131.16 (**B**), and ^{15}N-labled sample from the clade C isolate 92BR025.9 (with M687K mutation) (**C**). All spectra were recorded at ^{1}H frequency of 600 MHz. Assignment of backbone amide resonances are shown for gp41(677-716) from clade D 92UG024.2 (gp41$^{\text{HIV1D (677-716)}}$).

Fig. S4

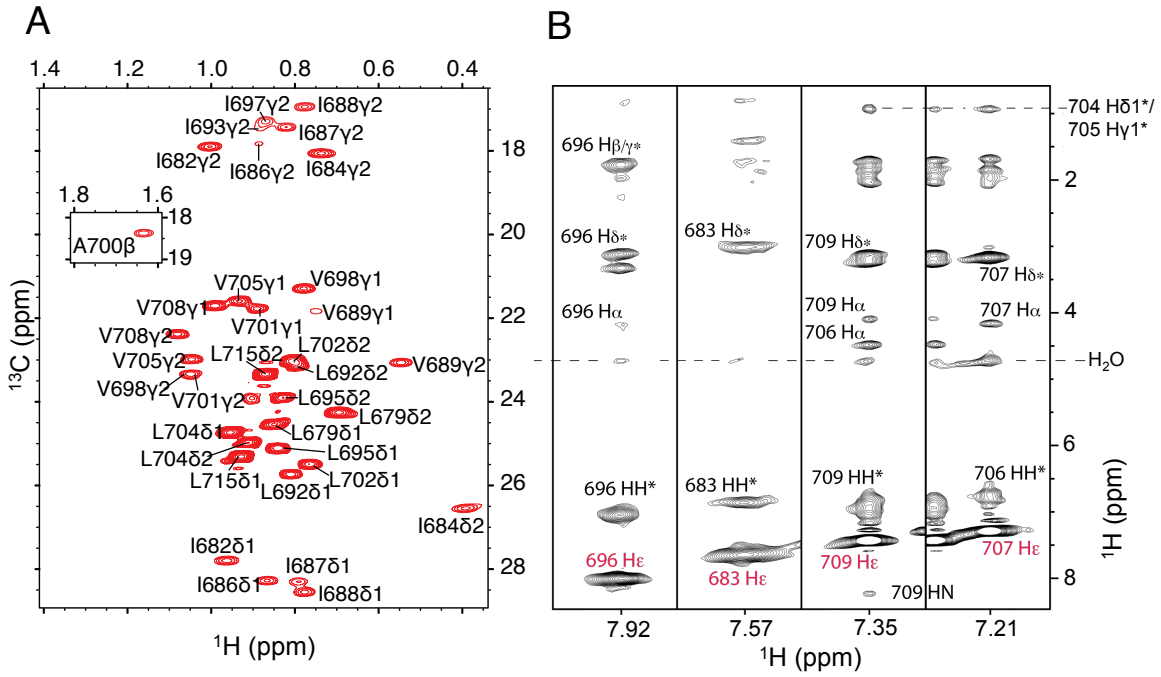

Figure S4. NMR spectra of gp41$^{HIV1D\ (677-716)}$ sidechain groups. (A) The 2D ^{1}H-^{13}C HSQC (28 ms ^{13}C constant time) recorded at 900 MHz showing the assignments of methyl group resonances of gp41$^{HIV1D\ (677-716)}$ trimer in bicelles (with deuterated DMPC and DHPC). **(B)** NOE strips of the four Arg side chain epsilon protons from the 3D ^{15}N-edited NOESY-TROSY-HSQC spectrum. The spectrum was recorded with NOE mixing time of 60 ms at ^{1}H frequency of 600 MHz. The sample used consists of uniformly (^{15}N, ^{13}C)-labeled protein reconstituted in DMPC/DHPC bicelles (q = 0.5), in which the acyl chains of DMPC and DHPC were deuterated. The assignments of the diagonal peaks are shown in red.

Fig. S5

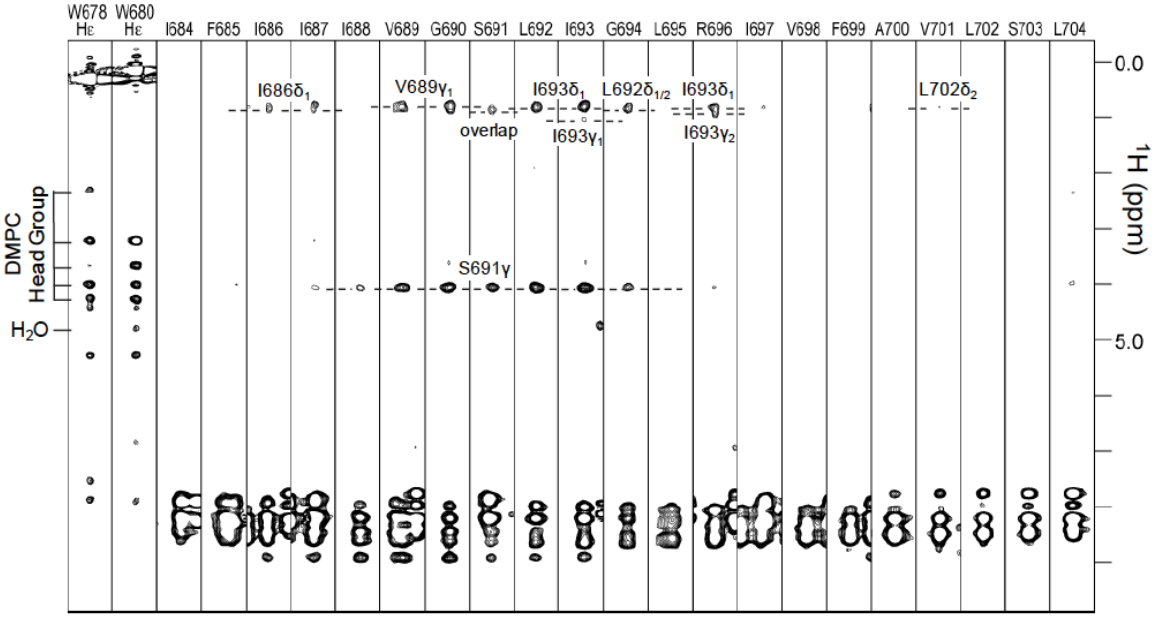

Figure S5. Intermonomer NOEs from the mixed isotope labeled gp41$^{HIV1D(677-716)}$. Residue-specific strips taken from the 3D ^{15}N-edited NOESY-TROSY-HSQC spectrum (NOE mixing time = 300 ms) recorded at 750 MHz using the bicelle-reconstituted gp41$^{HIV1D(677-716)}$ sample containing 50% (^{15}N, ^{2}H)-labeled protein and 50% (15% ^{13}C)-labeled protein. The crosspeaks in the aliphatic regions are intermonomer NOEs between the backbone amide and the sidechain methyl protons. The strips corresponding to the indole amines of W678 and W680 show NOEs to almost all the protons of the non-deuterated phospholipid headgroup, suggesting that the tryptophans reside within the headgroup region of the bicelle. The methyl group chemical shifts in the TM region are very similar in the proton dimension. The methyl NOE crosspeaks were initially assigned based on the assumption that the three equivalent TM helices form parallel trimers, i.e., intermonomer NOEs can only be between residues that are nearby along the amino acid sequence. These NOE assignments were subsequently validated and complemented by self-consistent NOEs from the ^{13}C- and ^{15}N-edited NOESYs (900 MHz) of a uniformly (^{15}N, ^{13}C)-labeled sample.

Fig. S6

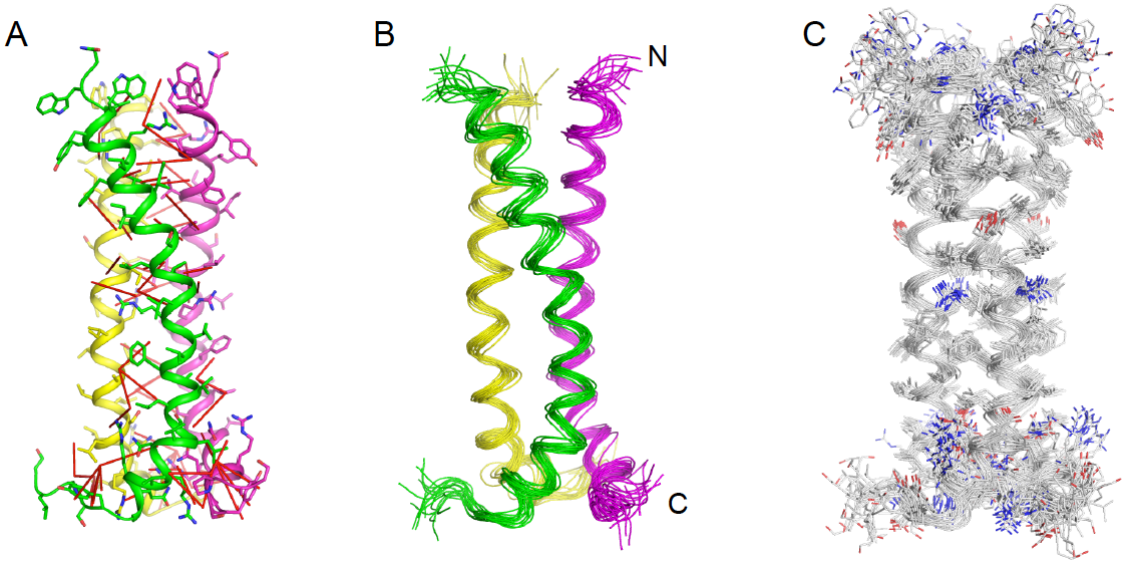

Figure S6. Structures of gp41$^{HIV1D(677-716)}$ calculated with NMR restraints. (A) Ribbon representation of the trimer structure showing NOE-derived intermonomer restraints (red lines). **(B)** Ensemble of 15 lowest energy structures calculated using NMR-derived structural restraints (see Table S1). Structures are shown as thin ribbon representation of the backbones. **(C)** Same as in (B) but includes the side chains.

Fig. S7

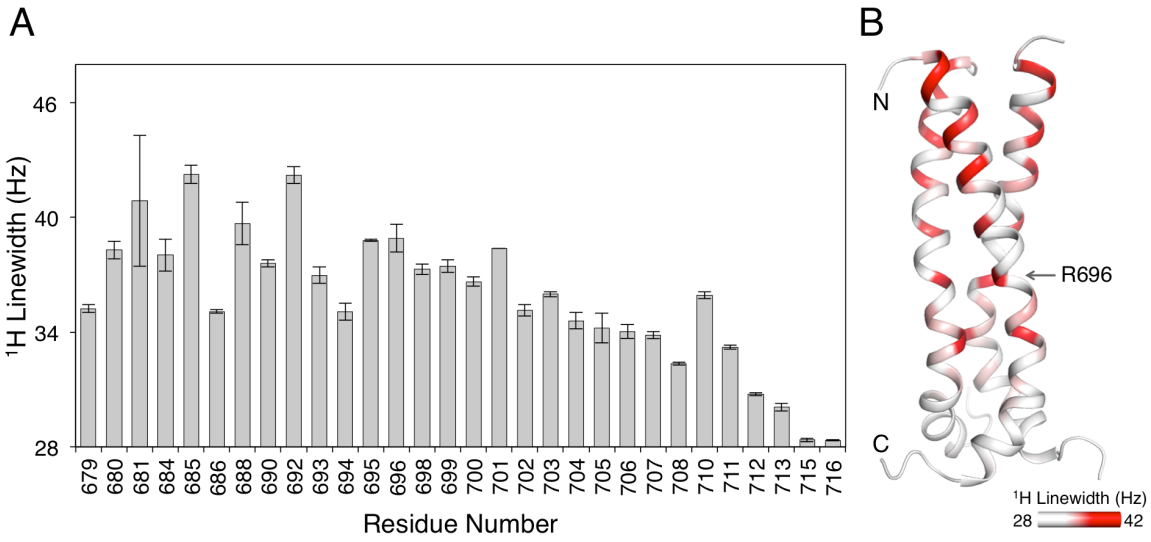

Figure S7. ^{1}H linewidth for backbone amide resonances of gp41$^{HIV1D(677-716)}$. (A) Residue-specific ^{1}H linewidth of the backbone amide resonances of gp41$^{HIV1D(677-716)}$ derived from the ^{1}H-^{15}N TROSY-HSQC spectrum of a (^{2}H,^{15}N,^{13}C)-labeled sample, recorded at 750 MHz. The ^{1}H linewidths were determined using NMRDraw and overlapped resonances were not analyzed. Mean ^{1}H linewidths from two spectra are plotted in the graph, with error bars representing the standard deviation. The ^{1}H linewidths of the N-terminal half of the protein (residues 679-696) are significantly larger (P=0.0007, two-tailed unpaired T test) than those of the C-terminal half (residues 698-712). **(B)** Mapping of ^{1}H linewidth from (A) onto the gp41$^{HIV1D(677-716)}$ structure.

Fig. S8

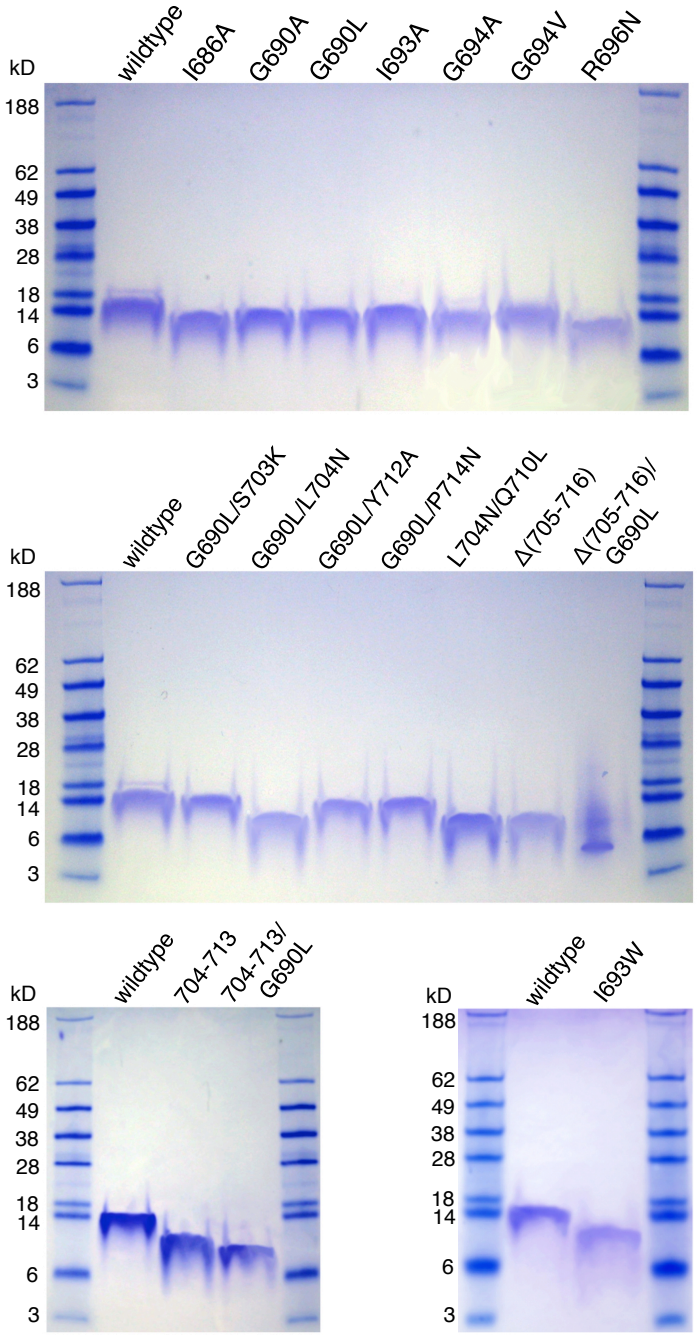

Figure S8. SDS-PAGE analysis of purified and reconstituted gp41$^{HIV1D(677-716)}$ mutants. gp41$^{HIV1D(677-716)}$ mutants were purified in the same way as the wildtype protein (described in Materials and Methods), reconstituted in bicelles and analyzed by SDS-

PAGE under non-boiling conditions. For the 704-713 mutant, the sequence of residues 704-713 (VINRVRQGYS) was mutated to SSAASAAGSA.

Fig. S9

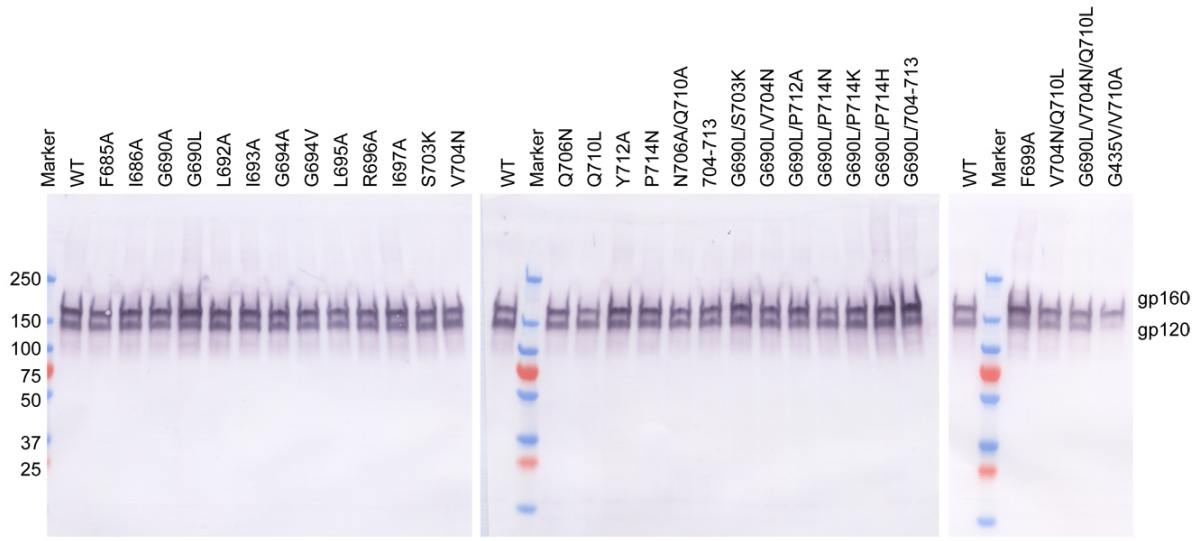

Figure S9. Expression and processing of Env mutants expressed in 293T cells. Env samples prepared from 293T cells transiently transfected with 5 μg of the HIV-1 gp92UG037.8 gp160 expression plasmid or each of Env mutants were detected by an anti-V3 antibody 3791. The low level of cleavage of the mutant G435V/V710A may account for its low cell-cell fusion activity and lack of active pseudovirus.

Fig. S10

A

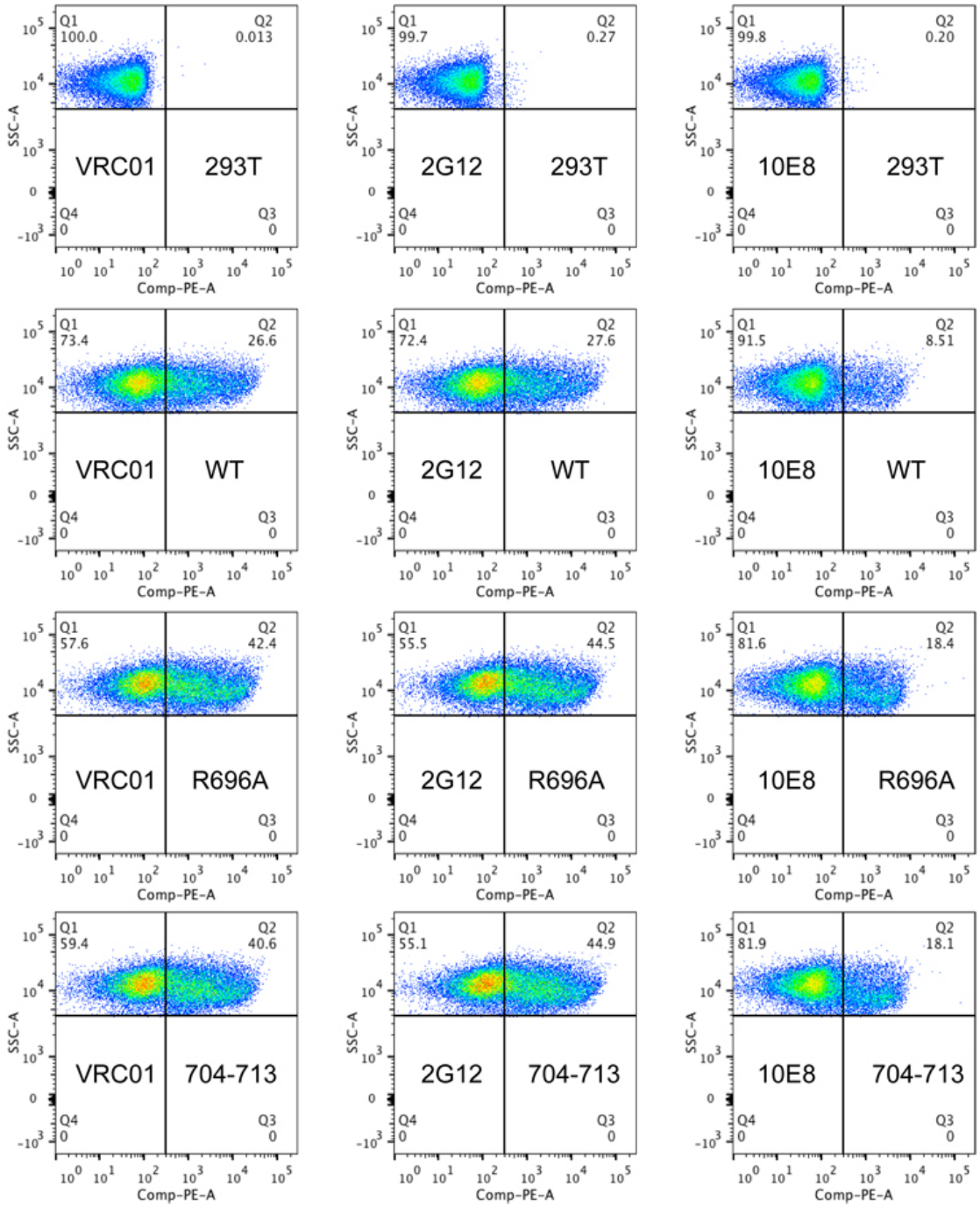
Q1 100.0
Q2 0.013
VRC01
293T
Q4 0
Q3 0
Q1 99.7
Q2 0.27
2G12
293T
Q4 0
Q3 0
Q1 99.8
Q2 0.20
10E8
293T
Q4 0
Q3 0
Q1 73.4
Q2 26.6
VRC01
WT
Q4 0
Q3 0
Q1 72.4
Q2 27.6
2G12
WT
Q4 0
Q3 0
Q1 91.5
Q2 8.51
10E8
WT
Q4 0
Q3 0
Q1 57.6
Q2 42.4
VRC01
R696A
Q4 0
Q3 0
Q1 55.5
Q2 44.5
2G12
R696A
Q4 0
Q3 0
Q1 81.6
Q2 18.4
10E8
R696A
Q4 0
Q3 0
Q1 59.4
Q2 40.6
VRC01
704-713
Q4 0
Q3 0
Q1 55.1
Q2 44.9
2G12
704-713
Q4 0
Q3 0
Q1 81.9
Q2 18.1
10E8
704-713
Q4 0
Q3 0
SSC-A
Comp-PE-A

B

Mutation	Mean Fluorescence Intensity (MFI)		
	2G12	**VRC01**	**10E8**
wildtype	1211	1046	193
F685A	1430	1206	319
I686A	1311	1084	229
G690A	1762	1488	389
G690L	1443	1215	214
L692A	1833	1529	325
I693A	1547	1242	302
G694A	1602	1400	349
G694V	1633	1343	332
L695A	1731	1387	340
R696A	2099	1793	390
I697A	1892	1623	409
F699A	1882	1629	210
S703K	2084	1803	476
V704N	2265	1877	532
N706A	1387	1165	160
Q710L	1821	1499	353
Y712A	2614	2150	353
P714N	2388	1940	384
N706A/Q710A	1797	1547	347
704-713	2043	1730	369
G690L/S703K	2144	1838	401
G690L/V704N	1802	1541	361
G690L/Y712A	2113	1817	329
G690L/P714N	2034	1694	323
G690L/P714K	2220	1783	449
G690L/P714H	2099	2019	234
G690/704-713	2616	1577	221
V704N/Q710L	1757	1599	406
G690L/V704N/Q710L	1292	1130	173
G435V/Q710A	1112	895	254
293T cell control	27	25	29

Figure S10. Cell-surface expression of Env mutants detected by flow cytometry. (A) Representative dot plots for negative control 293T cells, cells expressing the wildtype Env (WT), or mutants R696A and 704-713, measured by flow cytometry using monoclonal antibodies 2G12, VRC01 and 10E8. **(B)** Summary of mean fluorescence intensity (MFI) from data as shown in (A) for the wildtype and 30 Env mutants, as well as the 293T cell control.

Fig. S11

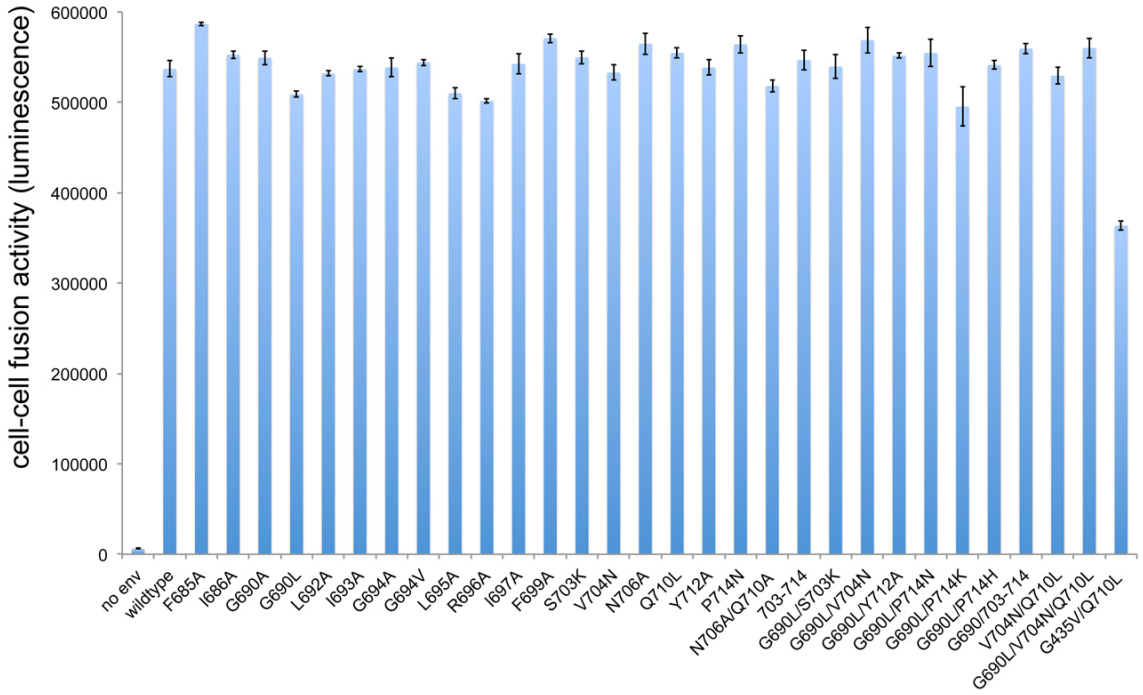

Figure S11. Cell-cell fusion of HIV-1 Env and its TMD mutants at a high expression level. 293T cells transfected with 5 μg of the 92UG037.8 Env expression plasmid or each of its TMD mutants were fused with CD4- and CCR5-expressing cells. Cell-cell fusion led to reconstitution of active β-galactosidase and thus the fusion activity was quantified by a chemiluminescent assay. No env was a negative control. The experiment was carried out in triplicate and repeated at least twice with similar results. Error bars indicate the standard deviation calculated by the Excel STDEV function. Data points are means ± standard deviations from triplicate measurements. Under these conditions, cell-cell fusion was not sensitive to inhibition by many neutralizing antibodies, such as PG9, PG16 and PGT145 (data not shown).

Fig. S12

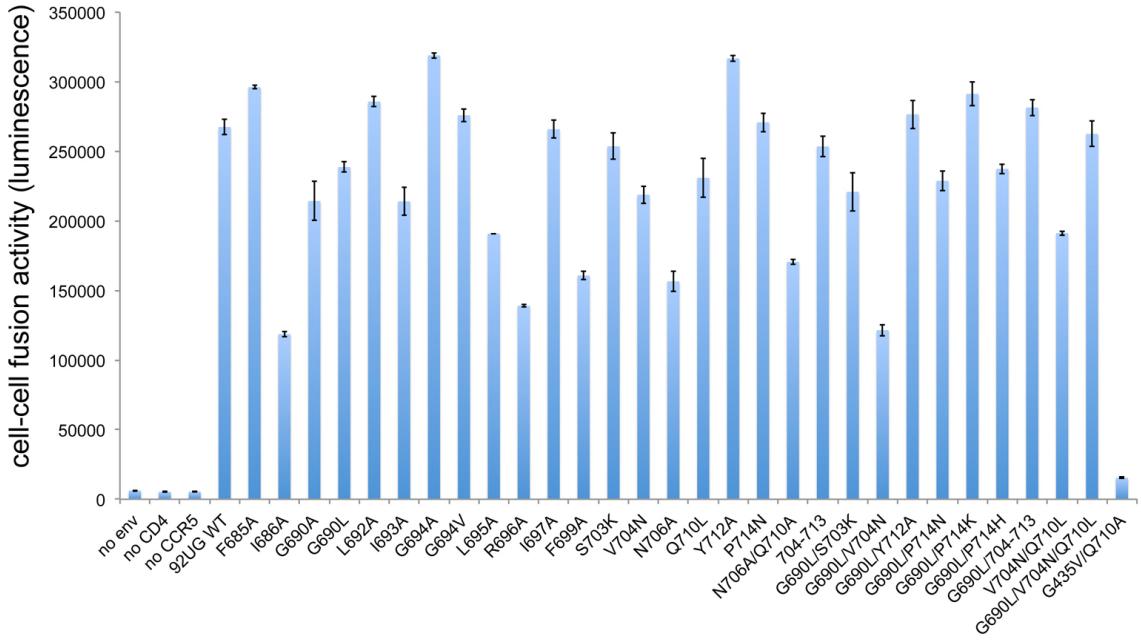

Figure S12. Cell-cell fusion of HIV-1 Env and its TMD mutants at a low expression level. 293T cells transfected with 25 ng of the 92UG037.8 Env expression plasmid or each of its TMD mutants were mixed with CD4- and CCR5-expressing cells. Cell-cell fusion led to reconstitution of active β-galactosidase and thus the fusion activity was quantified by a chemiluminescent assay. No env, no CD4 and no CCR5 were negative controls. The experiment was carried out in triplicate and repeated at least twice with similar results. Error bars indicate the standard deviation calculated by the Excel STDEV function. Data points are means ± standard deviations from triplicate measurements. The data are also summarized in Table S2.

Fig. S13

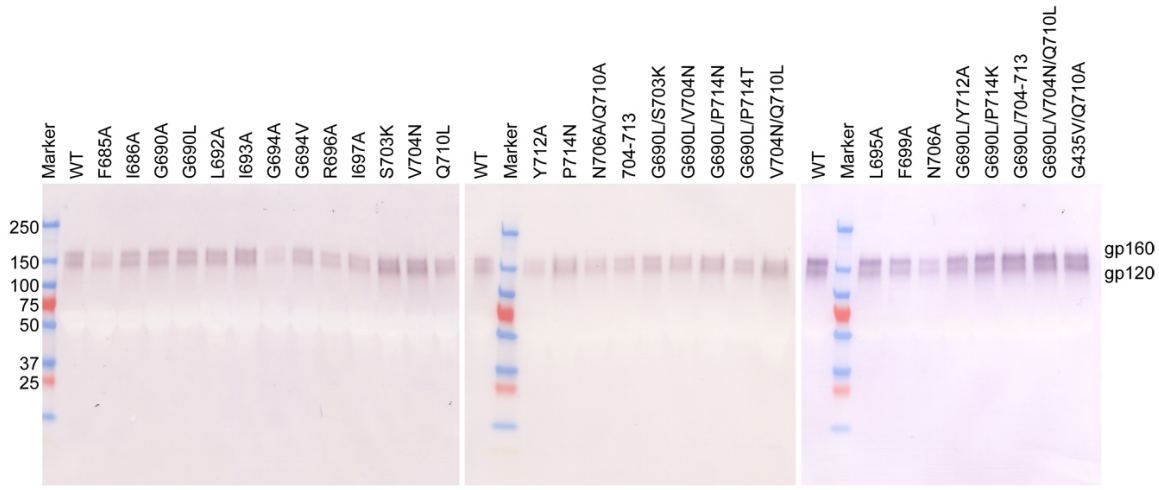

Figure S13. Incorporation of Env mutants into pseudoviruses analyzed by western blot. Env samples prepared from p24-normalized pseudoviruses containing either HIV-1 gp92UG037.8 Env or each of its TMD mutants were detected by an anti-V3 antibody 3791.

Fig. S14

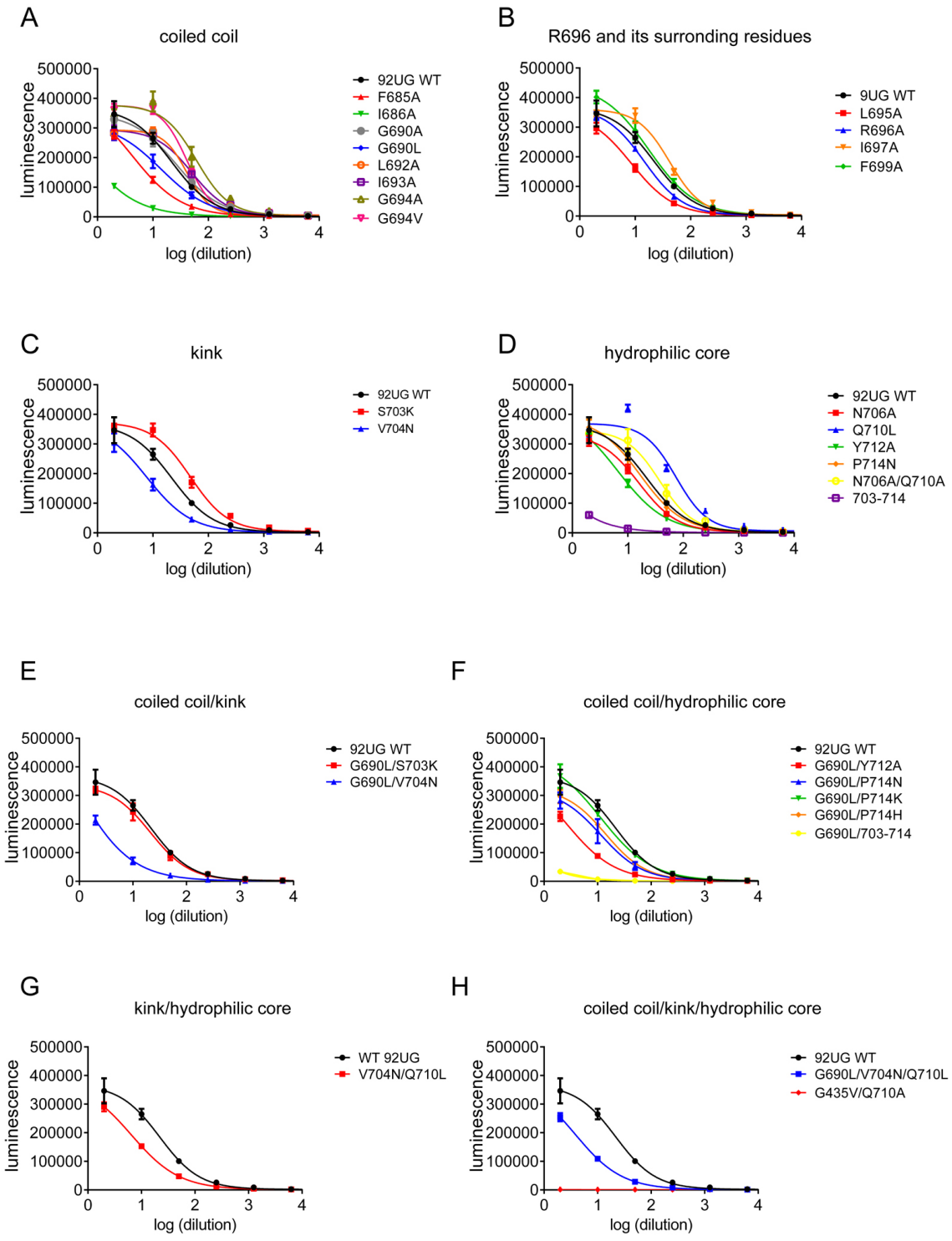

Figure S14. Viral infectivity of Env mutants. Pseudoviruses containing Env mutants were normalized by p24-antigen, titrated 10 times using 5-fold dilution series, and tested

for viral infectivity in TZM.bl cells. The Env mutants are grouped in (**A**) for those containing mutations in the coiled-coil; in (**B**) containing mutations of R696 and its surrounding residues; in (**C**) containing mutations in the kink; in (**D**) with mutations in the hydrophilic core; in (**E**) with mutations in the coiled-coil and kink; in (**F**) with mutations in the coiled-coil and hydrophilic core; in (**G**) with mutations in the kink and hydrophilic core; and in (**H**) with mutations in the coiled-coil, kink and hydrophilic core. The experiment was carried out in quadruplicate. Error bars indicate the standard deviation calculated by GraphPad Prism (GraphPad Software, Inc., La Jolla, CA).

Fig. S15 (A-B)

A. Analysis of mutations in the coiled coil of TMD

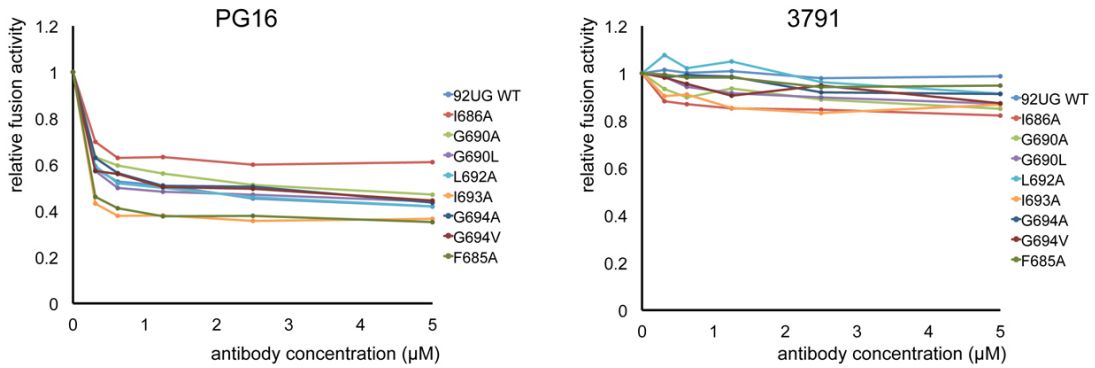

B. Analysis of mutations of R696 and its surrounding residues of TMD

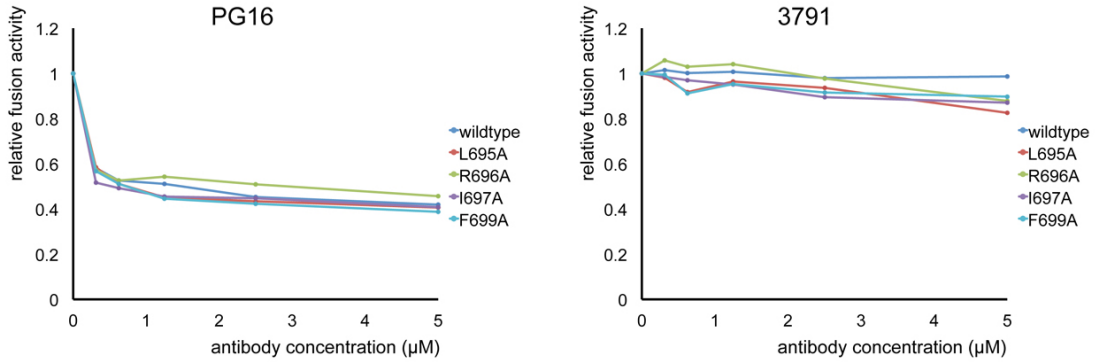

Fig. S15 (C-D)

C. Analysis of mutations in the kink of TMD

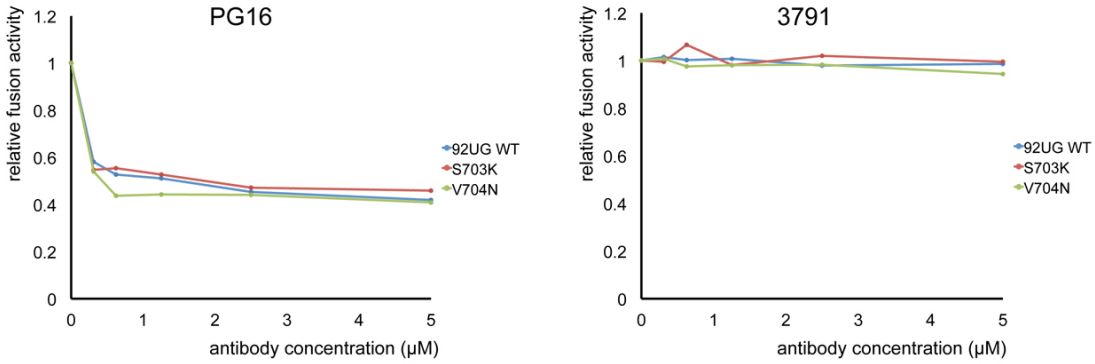

D. Analysis of mutations in the hydrophilic core of TMD

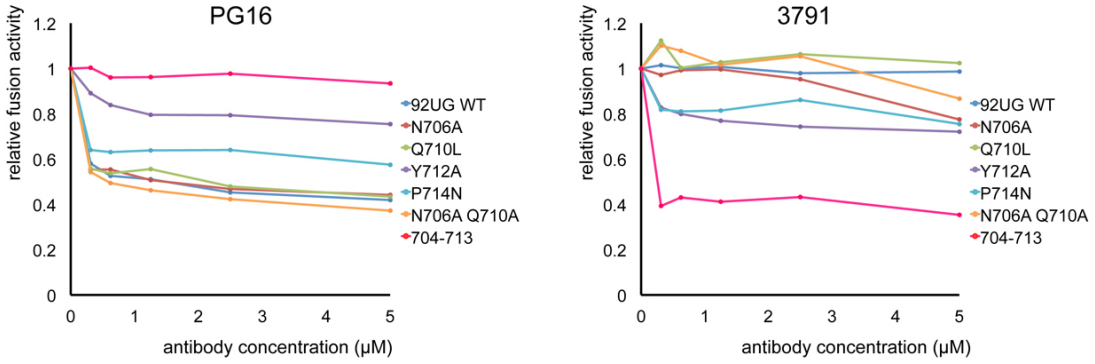

Fig. 15(E-F)

E. Analysis of mutations in the coiled coil/kink of TMD

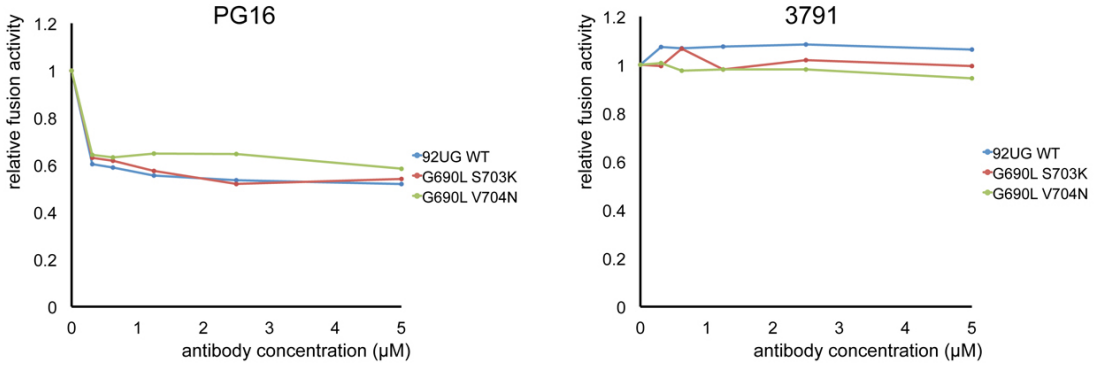

F. Analysis of mutations in the coiled coil/hydrophilic core of TMD

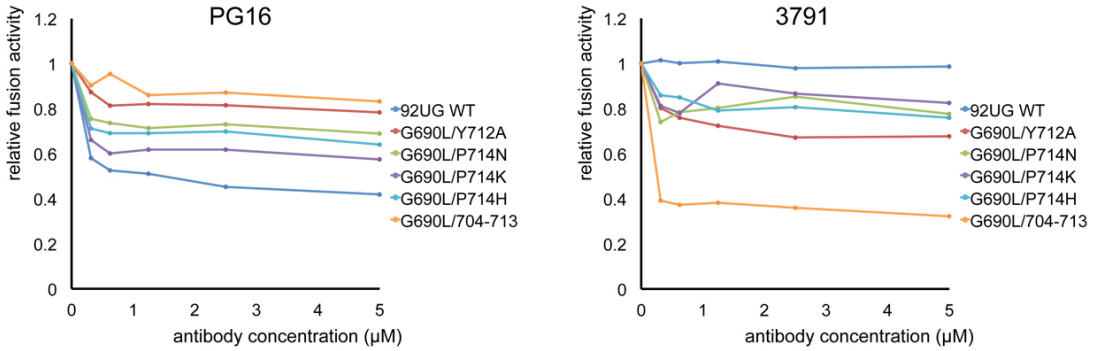

Fig. S15 (G-H)

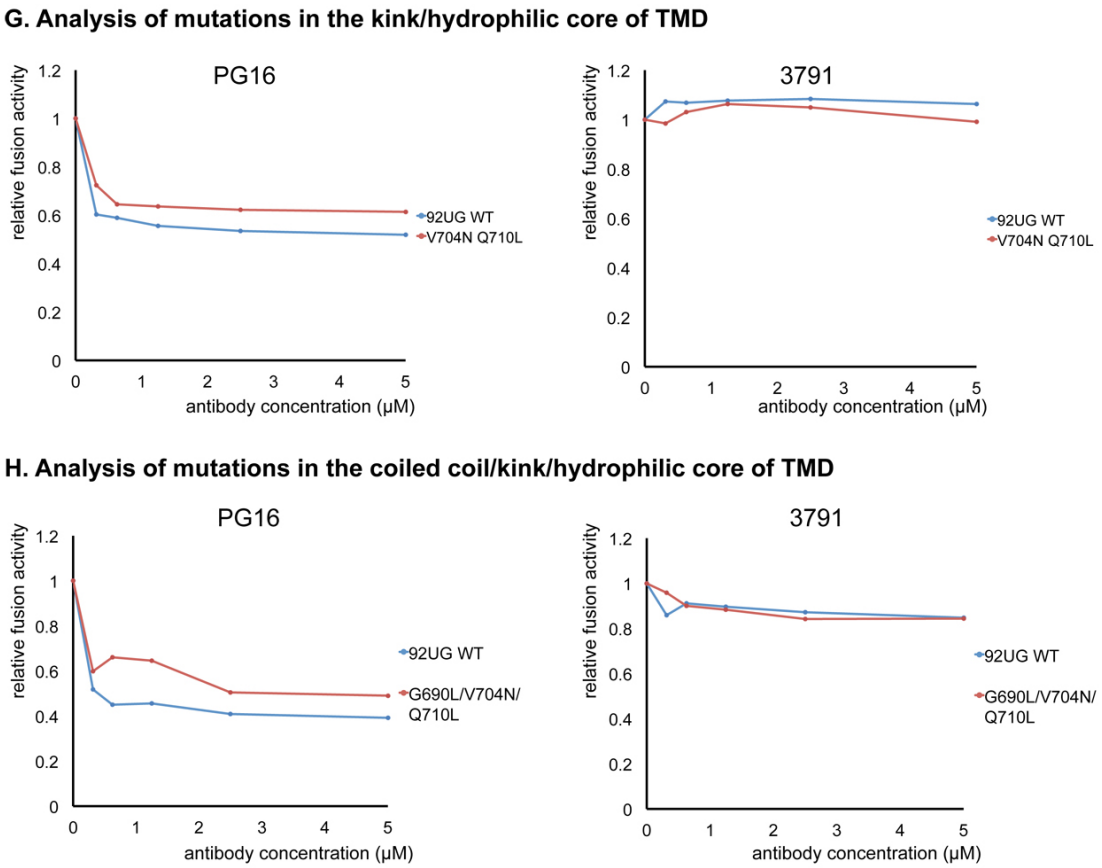

Figure S15. Antibody inhibition of cell-cell fusion mediated by the Env TMD mutants. The trimer-specific bnAb PG16 and non-neutralizing anti-V3 antibody 3791 were used to assess effect of mutations in various structural elements in the TMD on antibody inhibition of Env-mediated cell-cell fusion. The Env mutants are grouped in (**A**) for those containing mutations in the coiled-coil; in (**B**) containing mutations of R696 and its surrounding residues; in (**C**) containing mutations in the kink; in (**D**) with mutations in the hydrophilic core; in (**E**) with mutations in the coiled-coil and kink; in (**F**) with mutations in the coiled-coil and hydrophilic core; in (**G**) with mutations in the kink and hydrophilic core; and in (**H**) with mutations in the coiled-coil, kink and hydrophilic core. The experiment was carried out in duplicate and repeated at least twice with similar results.

Fig. S16

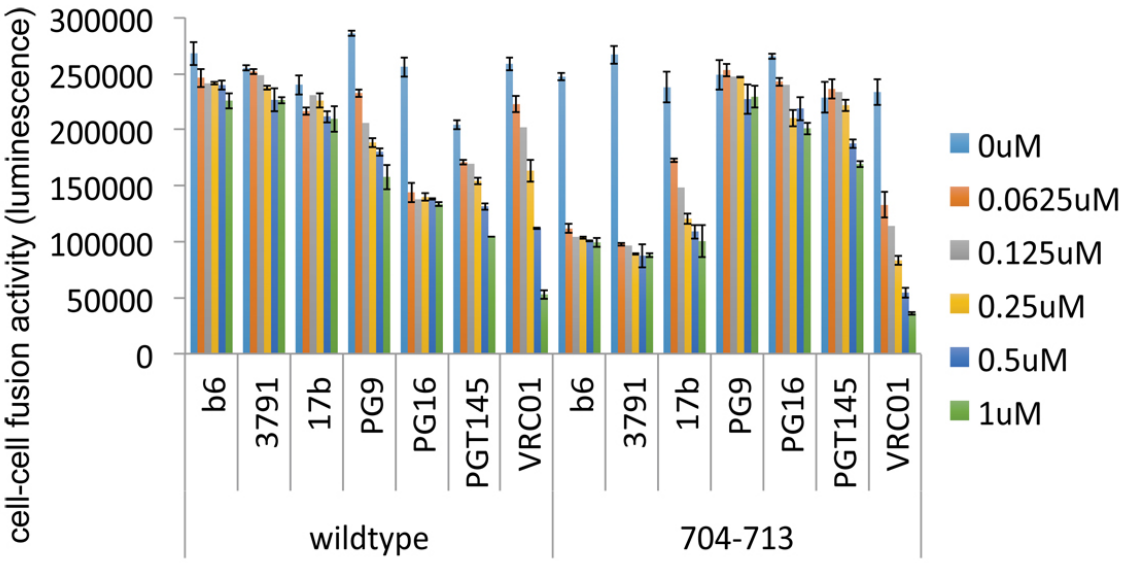

Figure S16. Antibody inhibition of cell-cell fusion mediated by the WT Env and mutant 704-713. Cell-cell fusion mediated by the wildtype 92UG037.8 Env (left) or the mutant 704-713 (right) was inhibited by non-neutralizing antibodies b6 (CD4 binding site), 3791 (V3) and 17b (CD4-induced), and trimer-specific bnAbs, PG9, PG16 and PGT145, respectively. The CD4 binding site bnAb VRC01 was a control antibody. The experiment was carried out in triplicate and repeated at least twice with similar results. Error bars indicate the standard deviation calculated by the Excel STDEV function. The data were summarized in Figure 3A.

Fig. S17

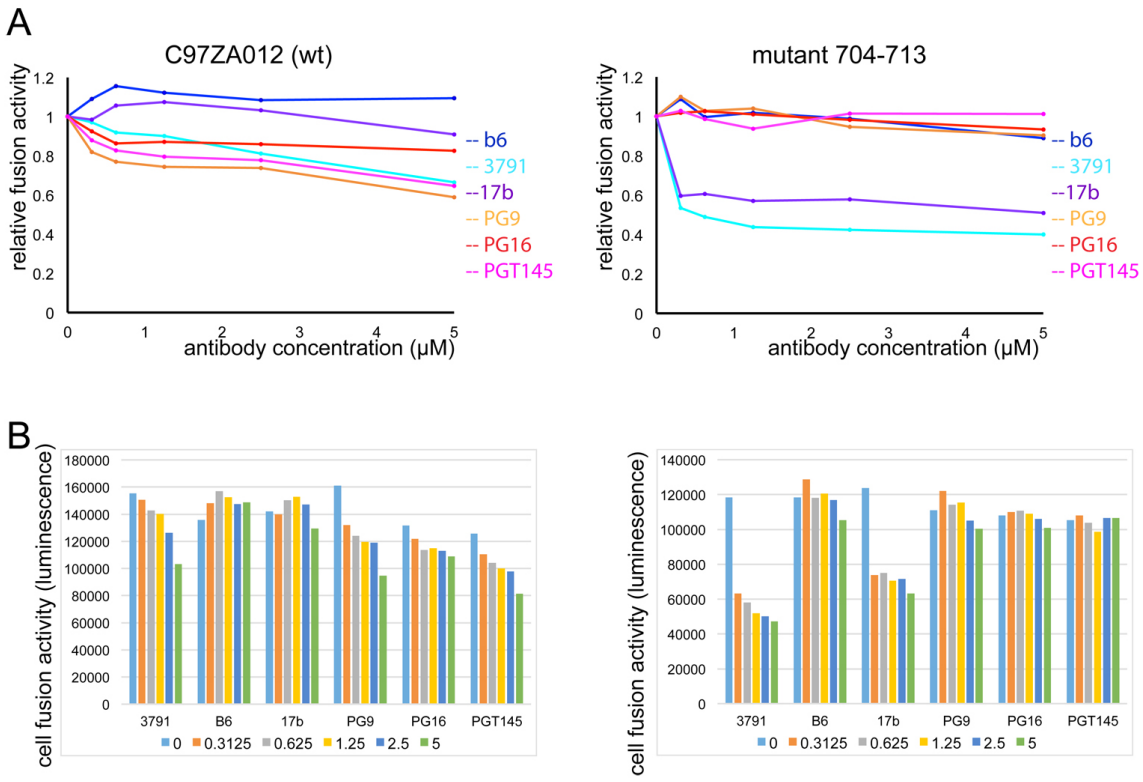

Figure S17. Antibody inhibition of cell-cell fusion mediated by the WT Env and mutant 704-713 derived from a clade C HIV-1 isolate C97ZA012. (**A**) Antibody inhibition of cell-cell fusion mediated by the wildtype C97ZA012 Env (left) and its TMD mutant 704-713 (right; residues 704-713 (IVNRVRQGYS) were mutated to SSAASAAGSA.) was analyzed using both non-neutralizing antibodies, including b6 (CD4 binding site; blue), 3791 (V3; cyan) and 17b (CD4-induced; purple), and trimer-specific bnAbs, including PG9 (orange), PG16 (red) and PGT145 (magenta). The C97ZA012 Env is totally resistant to antibody b6. The experiment was carried out in duplicate and repeated twice. (**B**) Raw data for (A).

Fig. S18

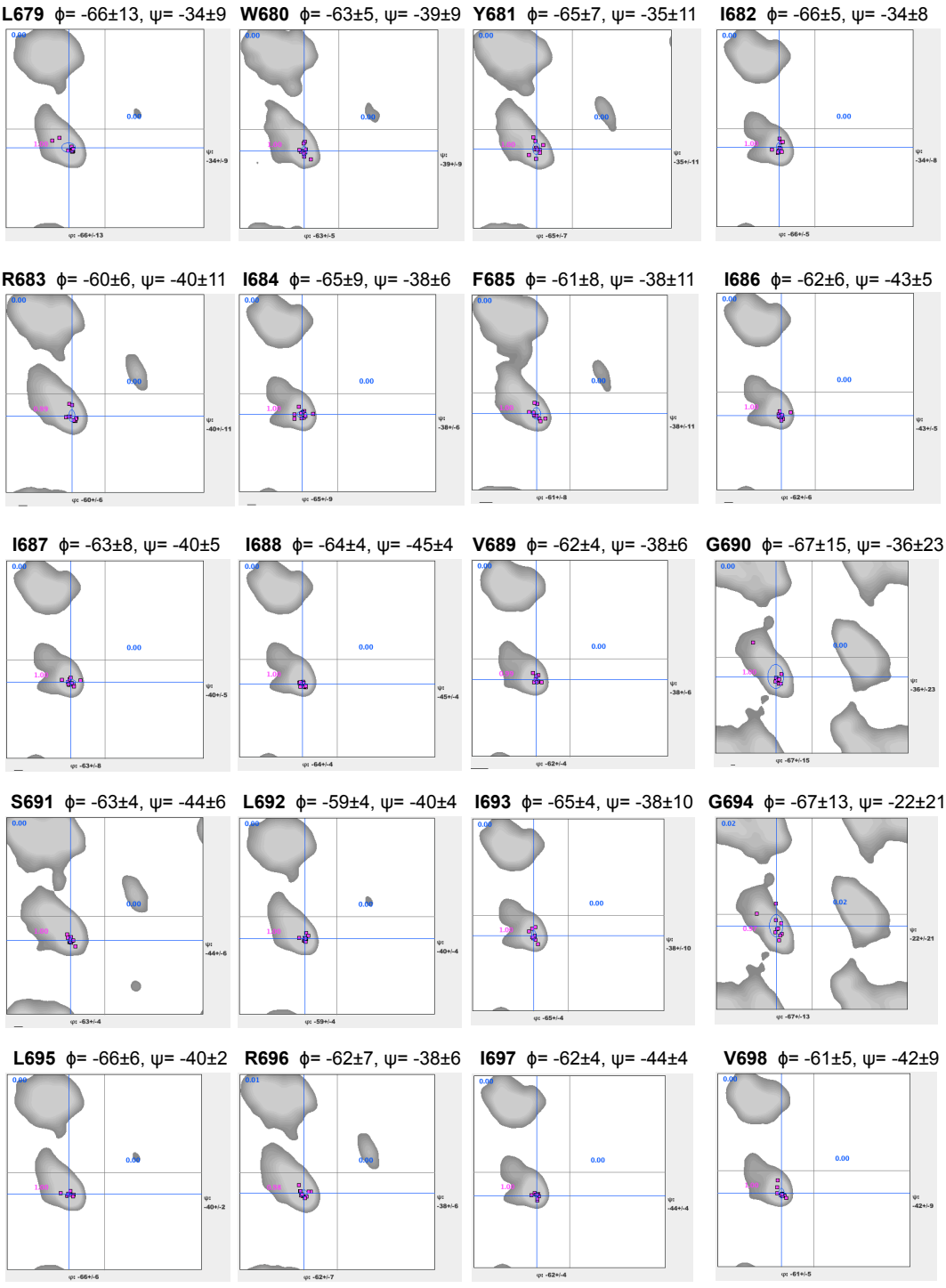
L679 ϕ= -66±13, ψ= -34±9
W680 ϕ= -63±5, ψ= -39±9
Y681 ϕ= -65±7, ψ= -35±11
I682 ϕ= -66±5, ψ= -34±8
R683 ϕ= -60±6, ψ= -40±11
I684 ϕ= -65±9, ψ= -38±6
F685 ϕ= -61±8, ψ= -38±11
I686 ϕ= -62±6, ψ= -43±5
I687 ϕ= -63±8, ψ= -40±5
I688 ϕ= -64±4, ψ= -45±4
V689 ϕ= -62±4, ψ= -38±6
G690 ϕ= -67±15, ψ= -36±23
S691 ϕ= -63±4, ψ= -44±6
L692 ϕ= -59±4, ψ= -40±4
I693 ϕ= -65±4, ψ= -38±10
G694 ϕ= -67±13, ψ= -22±21
L695 ϕ= -66±6, ψ= -40±2
R696 ϕ= -62±7, ψ= -38±6
I697 ϕ= -62±4, ψ= -44±4
V698 ϕ= -61±5, ψ= -42±9

Fig. S18 (continued)

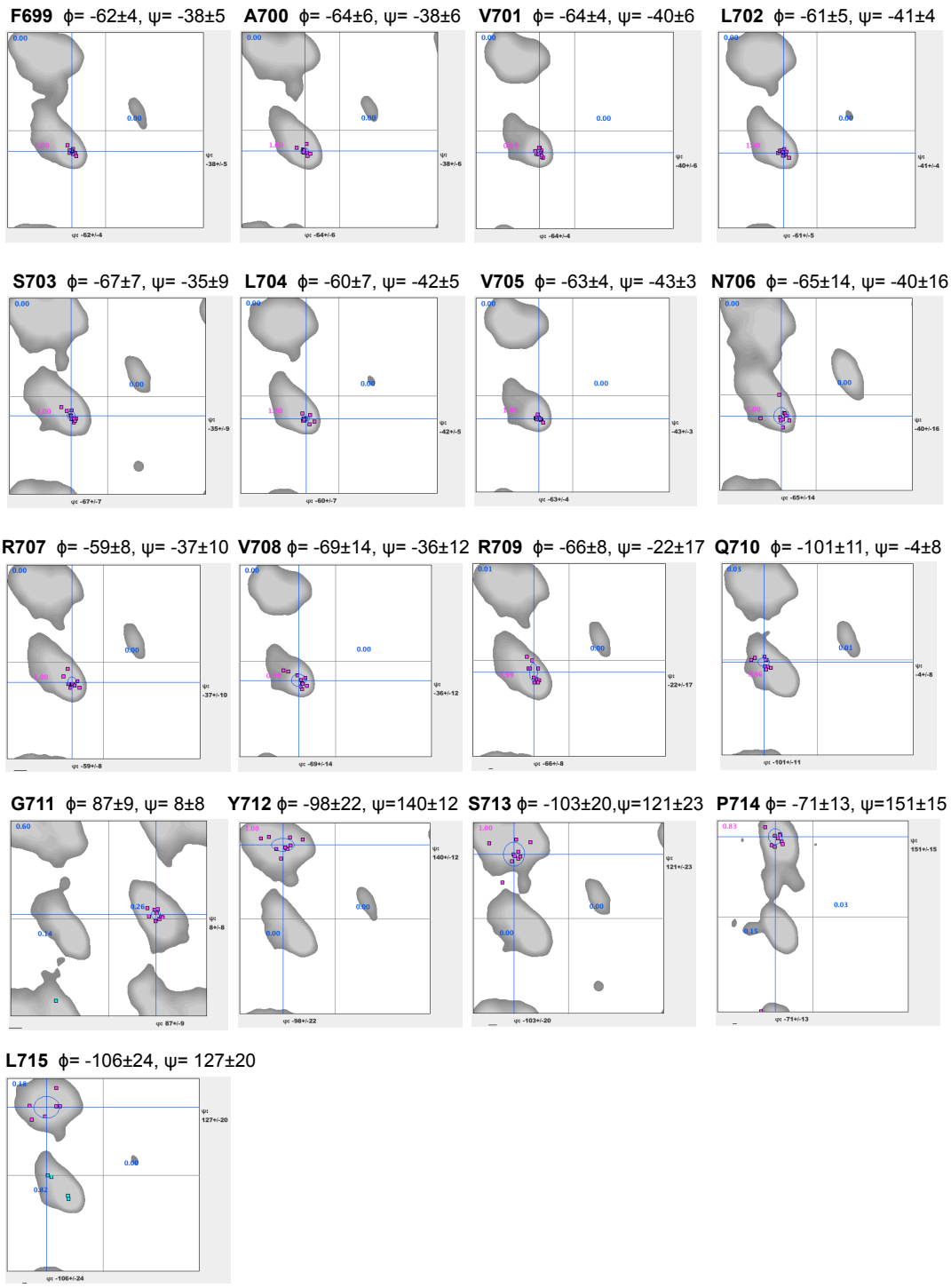

Figure S18. **Backbone dihedral angles of residues in gp41$^{HIV1D(677-716)}$.** Ramachandran plots showing the backbone dihedral angles, ϕ and ψ, and their respective uncertainties. The dihedrals were derived by TALOS+ using N, Cα, and C' chemical shifts. Among the

residues analyzed, all except G711 and L715 were considered “Good” by TALOS+. The Good dihedral angles and uncertainties were used as restraints in XPLOR calculation.

Fig. S19

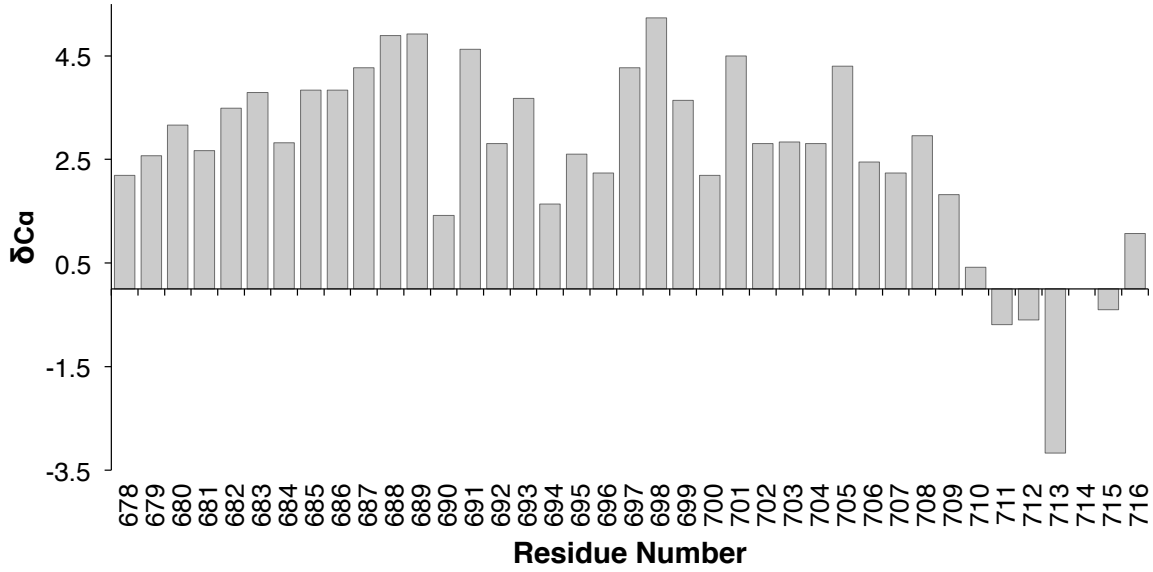

Figure S19. Backbone secondary Cα chemical shifts for each residue. The difference between backbone Cα chemical shifts (of each amino acid in $gp41^{HIV1D(677\text{-}716)}$) to the random coil Cα chemical shift is plotted as the secondary Cα chemical shift. The random coil Cα values were obtained from the Biological Magnetic Resonance Data Bank (http://www.bmrb.wisc.edu/).

Fig. S20

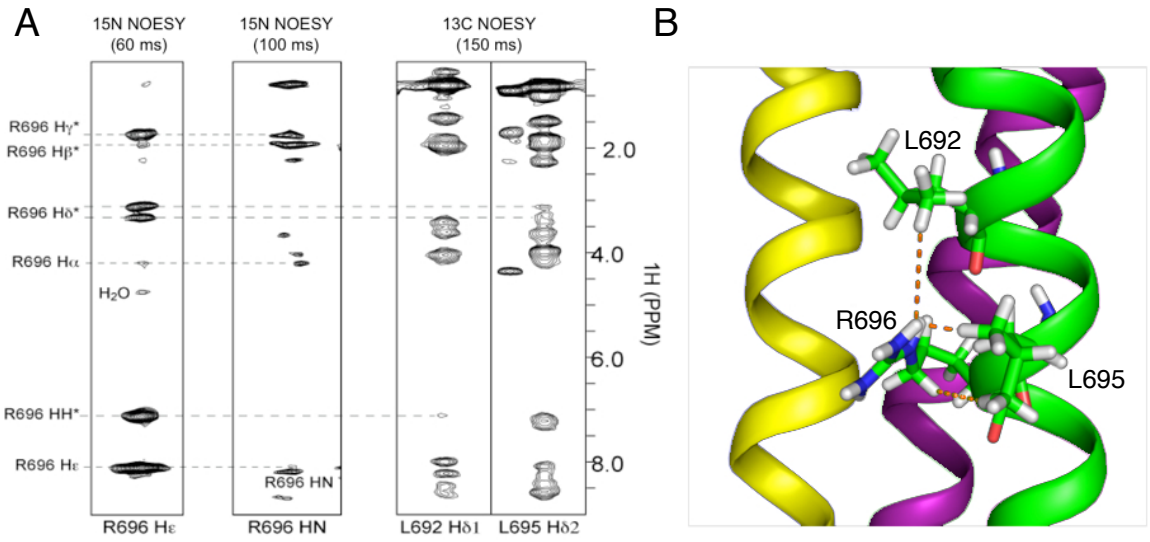

Figure S20. NOEs to the side chain of R696. (A) NOE strips from ^{15}N-edited and ^{13}C-edited NOESYs showing key NOEs that define the side chain conformation of R696. **(B)** Position of L695 and L692 with respect to R696.

Table S1

Table S1. NMR and refinement statistics

NMR distance and dihedral constraints [a]	
Distance constraints from NOE	585
Short-range intramolecular ($\|i-j\| \leq 4$)	498
Long-range intramolecular ($\|i-j\| \geq 5$)	3
Intermolecular	84
Total dihedral angle restraints [b]	210
ϕ (TALOS)	105
ψ (TALOS)	105
Structure statistics [c]	
Violations (mean ± s.d.)	
Distance constraints (Å)	0.217 ± 0.006
Dihedral angle constraints (º)	2.167 ± 0.108
Deviations from idealized geometry	
Bond lengths (Å)	0.033 ± 0.000
Bond angles (º)	1.669 ± 0.024
Impropers (º)	1.010 ± 0.025
Average pairwise r.m.s. deviation (Å) [d]	
Heavy	1.442
Backbone	0.946

[a] The numbers of constraints are summed over all three subunits. [b] The backbone dihedrals that were considered as "Good" by TALOS+ (*41*) were applied in structure calculation with uncertainties from TALOS+ (see Fig. S17). [c] Statistics are calculated and averaged over an ensemble of the 15 lowest energy structures out of 150 calculated structures. [d] The precision of the atomic coordinates is defined as the average r.m.s. difference between the 15 final structures and their mean coordinates.

Table S2

Table S2. Functional analysis of mutations in the HIV-1 TMD

Mutation	Structural element	Cell-cell fusion[a]	Viral infectivity[b]
wildtype	n/a	100.0±2.1	100.0±12.6
F685A	coiled-coil	110.7±0.5	80.2±3.5
I686A		44.3±0.7	30.2±0.2
G690A		80.1±5.3	95.0±3.2
G690L		89.3±1.3	80.6±4.6
L692A		106.8±1.4	81.2±2.8
I693A		80.0±3.8	81.8±5.9
G694A		119.2±0.7	100.2±4.5
G694V		103.2±1.7	104.3±5.9
L695A	R696 and its surrounding residues	71.4±0.0	85.6±5.1
R696A		52.0±0.6	97.3±3.7
I697A		99.4±2.4	99.8±3.0
F699A		60.1±1.1	115.8±7.2
S703K	kink	94.8±3.5	102.4±4.0
V704N		81.8±2.3	87.7±8.0
N706A	hydrophilic core	58.5±2.7	89.6±4.4
Q710L		86.3±5.2	90.5±2.9
Y712A		118.4±0.7	92.0±4.2
P714N		101.3±2.5	102.8±7.7
N706A/Q710A		63.8±0.6	96.6±2.4
704-713[c]		94.8±2.8	17.4±0.3
G690L/S703K	coiled-coil/kink	82.6±5.1	91.7±3.4
G690L/V704N		45.4±1.5	61.7±2.8
G690L/Y712A	coiled-coil/hydrophilic core	103.4±3.8	65.4±3.1
G690L/P714N		85.5±2.7	81.3±6.7
G690L/P714K		108.9±3.2	106.0±12.6
G690L/P714H		88.7±1.3	85.5±5.8
G690L/704-713		105.2±2.2	9.8±0.2
V704N/Q710L	kink/hydrophilic core	71.5±0.6	83.8±3.8
G690L/V704N/Q710L	coiled-coil/kink/hydrophilic core	98.2±3.3	73.3±3.0
G435V/Q710A[d]	gp120/gp41	5.8±0.2	<0.1

[a]Cell-cell fusion assay was performed in triplicate at a low Env expression level to mimic HIV-1 virions and the original data are shown in Figure S12. [b]Viral infectivity assay was performed in quadruplicate using p24-normalized pseudoviruses and titration data for each virus with 5-fold dilution series are also shown in Figure S14. [c]704-713, residues 704-713 (VINRVRQGYS) were mutated to SSAASAAGSA. [d]Mutant G435V/Q710A was created accidentally with a mutation in gp120 and used as a control. Data points are means ± standard deviations from triplicate measurements.

Table S3

Table S3. List of monoclonal antibodies targeting HIV-1 Env used in this study.

Epitope	antibody	reference
CD4 binding site	VRC01, 3BNC117 and b6	ref (*46*)
N160 glycan dependent, trimer-specific epitope	PG9, PG16 and PGT145	ref (*47, 48*)
N332 glycan dependent epitope	10-1074	ref (*49*)
CD4i epitope	17b	ref (*50*)
V3	3791	ref (*51*)
MPER	10E8	ref (*52*)

Table S4

Table S4. Antibody neutralization of Env mutants.

Mutant	3791			PG9			3BNC117			10-1074			10E8		
	IC_{50}	IC_{80}	MPI	IC_{50}	IC_{80}	MPI	IC_{50}	IC_{80}	MPI	IC_{50}	IC_{80}	MPI	IC_{50}	IC_{80}	MPI
wildtype	>50	>50	13	0.016	0.073	99	0.014	0.052	100	0.070	0.241	100	0.424	2.154	100
F685A	>50	>50	1	0.018	0.073	100	0.028	0.090	100	0.070	0.254	100	0.034	0.276	100
I686A	>50	>50	39	0.030	0.240	89	0.009	0.040	100	0.082	0.262	100	0.119	0.828	99
G690A	>50	>50	13	0.016	0.077	99	0.016	0.046	100	0.074	0.252	100	0.498	2.412	100
G690L	>50	>50	21	0.022	0.118	96	0.013	0.047	100	0.081	0.264	100	0.036	0.263	100
L692A	>50	>50	2	0.021	0.076	99	0.019	0.066	100	0.080	0.278	100	0.578	4.435	100
I693A	>50	>50	1	0.023	0.104	99	0.020	0.070	100	0.096	0.321	100	1.166	5.508	100
G694A	>50	>50	12	0.018	0.071	99	0.022	0.063	100	0.092	0.308	100	0.437	3.187	100
G694V	>50	>50	19	0.020	0.071	99	0.018	0.053	100	0.108	0.366	100	0.236	1.806	100
L695A	>50	>50	11	0.032	0.114	99	0.015	0.050	100	0.087	0.384	100	0.266	1.880	100
R696A	>50	>50	8	0.019	0.056	99	0.014	0.034	100	0.065	0.168	100	0.032	0.162	100
I697A	>50	>50	5	0.022	0.090	99	0.017	0.061	100	0.118	0.356	100	0.424	1.638	100
F699A	>50	>50	19	0.019	0.103	95	0.006	0.022	100	0.039	0.138	100	0.001	0.022	100
S703K	>50	>50	31	0.030	0.137	99	0.034	0.104	100	0.126	0.341	100	0.089	0.590	100
V704N	>50	>50	30	0.032	0.686	91	0.025	0.074	100	0.127	0.422	100	0.010	0.089	100
N706A	>50	>50	14	0.007	0.055	98	0.015	0.064	100	0.086	0.331	100	0.042	0.519	100
Q710L	>50	>50	16	0.014	0.097	99	0.020	0.075	100	0.117	0.417	100	0.049	0.433	100
Y712A	>50	>50	37	0.016	0.060	100	0.007	0.032	100	0.052	0.167	100	0.031	0.183	100
P714N	>50	>50	19	0.013	0.087	99	0.015	0.050	100	0.070	0.249	100	0.026	0.244	100
N706A/Q710A	>50	>50	1	0.021	0.119	98	0.019	0.069	100	0.145	0.490	100	0.385	2.498	100
704-713	1.594	>50	66	0.834	>50	68	0.007	0.029	100	0.095	0.257	100	0.004	0.041	100
G690L/S703K	>50	>50	19	0.022	0.169	96	0.010	0.045	100	0.074	0.258	100	0.017	0.126	100
G690L/V704N	>50	>50	44	0.044	18.130	81	0.012	0.042	100	0.102	0.337	100	0.013	0.053	100
G690L/Y712A	>50	>50	4	0.016	0.099	93	0.009	0.032	100	0.084	0.284	100	0.018	0.170	100
G690L/P714N	>50	>50	10	0.025	0.116	92	0.013	0.028	100	0.064	0.207	100	0.013	0.053	100
G690L/P714K	>50	>50	14	0.022	0.094	93	0.017	0.050	100	0.108	0.370	100	0.021	0.178	100
G690L/P714H	>50	>50	14	0.030	0.129	95	0.012	0.041	100	0.090	0.288	100	0.020	0.101	100
G690/704-713	0.016	>50	77	0.059	>50	63	<0.001	<0.001	100	0.041	0.155	100	0.002	0.024	100
V704N/Q710L	>50	>50	33	0.041	0.900	90	0.015	0.061	100	0.137	0.387	100	0.010	0.077	100
G690L/V704N/Q710L	35.223	>50	52	0.118	>50	77	0.022	0.061	100	0.139	0.457	100	0.008	0.084	100

References and Notes

1. S. C. Harrison, Viral membrane fusion. *Nat. Struct. Mol. Biol.* **15**, 690–698 (2008).doi:10.1038/nsmb.1456 Medline

2. D. C. Chan, D. Fass, J. M. Berger, P. S. Kim, Core structure of gp41 from the HIV envelope glycoprotein. *Cell* **89**, 263–273 (1997).doi:10.1016/S0092-8674(00)80205-6 Medline

3. W. Weissenhorn, A. Dessen, S. C. Harrison, J. J. Skehel, D. C. Wiley, Atomic structure of the ectodomain from HIV-1 gp41. *Nature* **387**, 426–430 (1997).doi:10.1038/387426a0 Medline

4. M. Pancera, T. Zhou, A. Druz, I. S. Georgiev, C. Soto, J. Gorman, J. Huang, P. Acharya, G. Y. Chuang, G. Ofek, G. B. Stewart-Jones, J. Stuckey, R. T. Bailer, M. G. Joyce, M. K. Louder, N. Tumba, Y. Yang, B. Zhang, M. S. Cohen, B. F. Haynes, J. R. Mascola, L. Morris, J. B. Munro, S. C. Blanchard, W. Mothes, M. Connors, P. D. Kwong, Structure and immune recognition of trimeric pre-fusion HIV-1 Env. *Nature* **514**, 455–461 (2014).doi:10.1038/nature13808 Medline

5. X. Wei, J. M. Decker, S. Wang, H. Hui, J. C. Kappes, X. Wu, J. F. Salazar-Gonzalez, M. G. Salazar, J. M. Kilby, M. S. Saag, N. L. Komarova, M. A. Nowak, B. H. Hahn, P. D. Kwong, G. M. Shaw, Antibody neutralization and escape by HIV-1. *Nature* **422**, 307–312 (2003).doi:10.1038/nature01470 Medline

6. D. D. Richman, T. Wrin, S. J. Little, C. J. Petropoulos, Rapid evolution of the neutralizing antibody response to HIV type 1 infection. *Proc. Natl. Acad. Sci. U.S.A.* **100**, 4144–4149 (2003).doi:10.1073/pnas.0630530100 Medline

7. J. H. Lee, G. Ozorowski, A. B. Ward, Cryo-EM structure of a native, fully glycosylated, cleaved HIV-1 envelope trimer. *Science* **351**, 1043–1048 (2016).doi:10.1126/science.aad2450 Medline

8. R. J. Owens, C. Burke, J. K. Rose, Mutations in the membrane-spanning domain of the human immunodeficiency virus envelope glycoprotein that affect fusion activity. *J. Virol.* **68**, 570–574 (1994). Medline

9. L. Shang, L. Yue, E. Hunter, Role of the membrane-spanning domain of human immunodeficiency virus type 1 envelope glycoprotein in cell-cell fusion and virus infection. *J. Virol.* **82**, 5417–5428 (2008).doi:10.1128/JVI.02666-07 Medline

10. L. Yue, L. Shang, E. Hunter, Truncation of the membrane-spanning domain of human immunodeficiency virus type 1 envelope glycoprotein defines elements required for fusion, incorporation, and infectivity. *J. Virol.* **83**, 11588–11598 (2009).doi:10.1128/JVI.00914-09 Medline

11. E. Helseth, U. Olshevsky, D. Gabuzda, B. Ardman, W. Haseltine, J. Sodroski, Changes in the transmembrane region of the human immunodeficiency virus type 1 gp41 envelope glycoprotein affect membrane fusion. *J. Virol.* **64**, 6314–6318 (1990). Medline

12. M. G. Teese, D. Langosch, Role of GxxxG Motifs in Transmembrane Domain Interactions. *Biochemistry* **54**, 5125–5135 (2015).doi:10.1021/acs.biochem.5b00495 Medline

13. J. Chen, J. M. Kovacs, H. Peng, S. Rits-Volloch, J. Lu, D. Park, E. Zablowsky, M. S. Seaman, B. Chen, Effect of the cytoplasmic domain on antigenic characteristics of HIV-1 envelope glycoprotein. *Science* **349**, 191–195 (2015).doi:10.1126/science.aaa9804 Medline

14. F. Gao, S. G. Morrison, D. L. Robertson, C. L. Thornton, S. Craig, G. Karlsson, J. Sodroski, M. Morgado, B. Galvao-Castro, H. von Briesen, S. Beddows, J. Weber, P. M. Sharp, G. M. Shaw, B. H. Hahn, Molecular cloning and analysis of functional envelope genes from human immunodeficiency virus type 1 sequence subtypes A through G. The WHO and NIAID Networks for HIV Isolation and Characterization. *J. Virol.* **70**, 1651–1667 (1996). Medline

15. J. F. Rowell, P. E. Stanhope, R. F. Siliciano, Endocytosis of endogenously synthesized HIV-1 envelope protein. Mechanism and role in processing for association with class II MHC. *J. Immunol.* **155**, 473–488 (1995). Medline

16. M. Boge, S. Wyss, J. S. Bonifacino, M. Thali, A membrane-proximal tyrosine-based signal mediates internalization of the HIV-1 envelope glycoprotein via interaction with the AP-2 clathrin adaptor. *J. Biol. Chem.* **273**, 15773–15778 (1998).doi:10.1074/jbc.273.25.15773 Medline

17. M. E. Call, J. R. Schnell, C. Xu, R. A. Lutz, J. J. Chou, K. W. Wucherpfennig, The structure of the zetazeta transmembrane dimer reveals features essential for its assembly with the T cell receptor. *Cell* **127**, 355–368 (2006).doi:10.1016/j.cell.2006.08.044 Medline

18. M. E. Call, K. W. Wucherpfennig, J. J. Chou, The structural basis for intramembrane assembly of an activating immunoreceptor complex. *Nat. Immunol.* **11**, 1023–1029 (2010).doi:10.1038/ni.1943 Medline

19. To produce the protein, we expressed the His-tagged TrpLE- gp41HIV1D(677-716) fusion protein in *Escherichia coli* as inclusion bodies, purified the solubilized protein by Ni-affinity chromatography, removed the TrpLE tag with cyanogen bromide, and separated the product by reverse-phasehigh-performance liquid chromatography. Bicelles were made of 1,2-dimyristoyl-sn-glycero-3-phosphocholine (DMPC; lipid) and 1,2-dihexanoyl-sn-glycero-3-phosphocholine (DHPC; detergent) at a ratio (*q*) of 0.5. In this report, we use gp41HIV1D(677–716) and TMD interchangeably for convenience.

20. K. J. Glover, J. A. Whiles, G. Wu, N. Yu, R. Deems, J. O. Struppe, R. E. Stark, E. A. Komives, R. R. Vold, Structural evaluation of phospholipid bicelles for solution-state studies of membrane-associated biomolecules. *Biophys. J.* **81**, 2163–2171 (2001).doi:10.1016/S0006-3495(01)75864-X Medline

21. C. R. Sanders 2nd, J. P. Schwonek, Characterization of magnetically orientable bilayers in mixtures of dihexanoylphosphatidylcholine and dimyristoylphosphatidylcholine by solid-state NMR. *Biochemistry* **31**, 8898–8905 (1992).doi:10.1021/bi00152a029 Medline

22. B. OuYang, S. Xie, M. J. Berardi, X. Zhao, J. Dev, W. Yu, B. Sun, J. J. Chou; B. OuYang, Unusual architecture of the p7 channel from hepatitis C virus. *Nature* **498**, 521–525 (2013).doi:10.1038/nature12283 Medline

23. For structure determination, we proceeded with the clade D construct because its expression level was the highest. The approach involves determination of local structures of the monomers and assembly of the trimer with intermonomer distance restraints derived from NOEs between structurally equivalent but isotopically differently labeled subunits. We could identify eight intermonomer NOEs using the isotopically mixed labeled sample to calculate a unique assembly solution, which was further validated and refined with other conventional NOE data.

24. Gd(DOTA) is a water-soluble and membrane-inaccessible molecule, so that the paramagnetic relaxation enhancement (PRE) it generates decreases with distance from the bilayer surface.

25. P. Zhu, J. Liu, J. Bess Jr., E. Chertova, J. D. Lifson, H. Grisé, G. A. Ofek, K. A. Taylor, K. H. Roux, Distribution and three-dimensional structure of AIDS virus envelope spikes. *Nature* **441**, 847–852 (2006).doi:10.1038/nature04817 Medline

26. R. W. Sanders, R. Derking, A. Cupo, J. P. Julien, A. Yasmeen, N. de Val, H. J. Kim, C. Blattner, A. T. de la Peña, J. Korzun, M. Golabek, K. de Los Reyes, T. J. Ketas, M. J. van Gils, C. R. King, I. A. Wilson, A. B. Ward, P. J. Klasse, J. P. Moore, A next-generation cleaved, soluble HIV-1 Env trimer, BG505 SOSIP.664 gp140, expresses multiple epitopes for broadly neutralizing but not non-neutralizing antibodies. *PLOS Pathog.* **9**, e1003618 (2013).doi:10.1371/journal.ppat.1003618 Medline

27. J. P. Julien, J. H. Lee, A. Cupo, C. D. Murin, R. Derking, S. Hoffenberg, M. J. Caulfield, C. R. King, A. J. Marozsan, P. J. Klasse, R. W. Sanders, J. P. Moore, I. A. Wilson, A. B. Ward, Asymmetric recognition of the HIV-1 trimer by broadly neutralizing antibody PG9. *Proc. Natl. Acad. Sci. U.S.A.* **110**, 4351–4356 (2013).doi:10.1073/pnas.1217537110 Medline

28. J. T. West, P. B. Johnston, S. R. Dubay, E. Hunter, Mutations within the putative membrane-spanning domain of the simian immunodeficiency virus transmembrane glycoprotein define the minimal requirements for fusion, incorporation, and infectivity. *J. Virol.* **75**, 9601–9612 (2001).doi:10.1128/JVI.75.20.9601-9612.2001 Medline

29. J. Chen, G. Frey, H. Peng, S. Rits-Volloch, J. Garrity, M. S. Seaman, B. Chen, Mechanism of HIV-1 neutralization by antibodies targeting a membrane-proximal region of gp41. *J. Virol.* **88**, 1249–1258 (2014).doi:10.1128/JVI.02664-13 Medline

30. C. Berlioz-Torrent, B. L. Shacklett, L. Erdtmann, L. Delamarre, I. Bouchaert, P. Sonigo, M. C. Dokhelar, R. Benarous, Interactions of the cytoplasmic domains of human and simian retroviral transmembrane proteins with components of the clathrin adaptor complexes modulate intracellular and cell surface expression of envelope glycoproteins. *J. Virol.* **73**, 1350–1361 (1999). Medline

31. S. A. Jeffs, S. Goriup, B. Kebble, D. Crane, B. Bolgiano, Q. Sattentau, S. Jones, H. Holmes, Expression and characterisation of recombinant oligomeric envelope glycoproteins derived from primary isolates of HIV-1. *Vaccine* **22**, 1032–1046 (2004).doi:10.1016/j.vaccine.2003.08.042 Medline

32. J. M. Kovacs, E. Noeldeke, H. J. Ha, H. Peng, S. Rits-Volloch, S. C. Harrison, B. Chen, Stable, uncleaved HIV-1 envelope glycoprotein gp140 forms a tightly folded trimer with a native-like structure. *Proc. Natl. Acad. Sci. U.S.A.* **111**, 18542–18547 (2014).doi:10.1073/pnas.1422269112 Medline

33. J. Guenaga, V. Dubrovskaya, N. de Val, S. K. Sharma, B. Carrette, A. B. Ward, R. T. Wyatt, Structure-guided redesign increases the propensity of HIV Env to generate highly stable soluble trimers. *J. Virol.* **90**, 2806–2817 (2015). Medline

34. Y. Do Kwon, M. Pancera, P. Acharya, I. S. Georgiev, E. T. Crooks, J. Gorman, M. G. Joyce, M. Guttman, X. Ma, S. Narpala, C. Soto, D. S. Terry, Y. Yang, T. Zhou, G. Ahlsen, R. T. Bailer, M. Chambers, G. Y. Chuang, N. A. Doria-Rose, A. Druz, M. A. Hallen, A. Harned, T. Kirys, M. K. Louder, S. O'Dell, G. Ofek, K. Osawa, M. Prabhakaran, M. Sastry, G. B. Stewart-Jones, J. Stuckey, P. V. Thomas, T. Tittley, C. Williams, B. Zhang, H. Zhao, Z. Zhou, B. R. Donald, L. K. Lee, S. Zolla-Pazner, U. Baxa, A. Schön, E. Freire, L. Shapiro, K. K. Lee, J. Arthos, J. B. Munro, S. C. Blanchard, W. Mothes, J. M. Binley, A. B. McDermott, J. R. Mascola, P. D. Kwong, Crystal structure, conformational fixation and entry-related interactions of mature ligand-free HIV-1 Env. *Nat. Struct. Mol. Biol.* **22**, 522–531 (2015).doi:10.1038/nsmb.3051 Medline

35. M. C. Wiener, S. H. White, Structure of a fluid dioleoylphosphatidylcholine bilayer determined by joint refinement of x-ray and neutron diffraction data. III. Complete structure. *Biophys. J.* **61**, 434–447 (1992).doi:10.1016/S0006-3495(92)81849-0 Medline

36. F. Delaglio, S. Grzesiek, G. W. Vuister, G. Zhu, J. Pfeifer, A. Bax, NMRPipe: A multidimensional spectral processing system based on UNIX pipes. *J. Biomol. NMR* **6**, 277–293 (1995).doi:10.1007/BF00197809 Medline

37. W. F. Vranken, W. Boucher, T. J. Stevens, R. H. Fogh, A. Pajon, M. Llinas, E. L. Ulrich, J. L. Markley, J. Ionides, E. D. Laue, The CCPN data model for NMR spectroscopy: Development of a software pipeline. *Proteins* **59**, 687–696 (2005).doi:10.1002/prot.20449 Medline

38. C. Bartels, T.-H. Xia, M. Billeter, P. Güntert, K. Wüthrich, The program XEASY for computer-supported NMR spectral analysis of biological macromolecules. *J. Biomol. NMR* **6**, 1–10 (1995).doi:10.1007/BF00417486 Medline

39. M. Salzmann, G. Wider, K. Pervushin, K. Wüthrich, Improved sensitivity and coherence selection for [15N,1H]-TROSY elements in triple resonance experiments. *J. Biomol. NMR* **15**, 181–184 (1999).doi:10.1023/A:1008358030477 Medline

40. C. D. Schwieters, J. J. Kuszewski, N. Tjandra, G. M. Clore, The Xplor-NIH NMR molecular structure determination package. *J. Magn. Reson.* **160**, 65–73 (2003).doi:10.1016/S1090-7807(02)00014-9 Medline

41. Y. Shen, F. Delaglio, G. Cornilescu, A. Bax, TALOS+: A hybrid method for predicting protein backbone torsion angles from NMR chemical shifts. *J. Biomol. NMR* **44**, 213–223 (2009).doi:10.1007/s10858-009-9333-z Medline

42. J. M. Kovacs, J. P. Nkolola, H. Peng, A. Cheung, J. Perry, C. A. Miller, M. S. Seaman, D. H. Barouch, B. Chen, HIV-1 envelope trimer elicits more potent neutralizing antibody responses than monomeric gp120. *Proc. Natl. Acad. Sci. U.S.A.* **109**, 12111–12116 (2012).doi:10.1073/pnas.1204533109 Medline

43. M. Li, F. Gao, J. R. Mascola, L. Stamatatos, V. R. Polonis, M. Koutsoukos, G. Voss, P. Goepfert, P. Gilbert, K. M. Greene, M. Bilska, D. L. Kothe, J. F. Salazar-Gonzalez, X. Wei, J. M. Decker, B. H. Hahn, D. C. Montefiori, Human immunodeficiency virus type 1 env clones from acute and early subtype B infections for standardized assessments of vaccine-elicited neutralizing antibodies. *J. Virol.* **79**, 10108–10125 (2005).doi:10.1128/JVI.79.16.10108-10125.2005 Medline

44. A. U. Holland, C. Munk, G. R. Lucero, L. D. Nguyen, N. R. Landau, Alpha-complementation assay for HIV envelope glycoprotein-mediated fusion. *Virology* **319**, 343–352 (2004).doi:10.1016/j.virol.2003.11.012 Medline

45. M. Sarzotti-Kelsoe, R. T. Bailer, E. Turk, C. L. Lin, M. Bilska, K. M. Greene, H. Gao, C. A. Todd, D. A. Ozaki, M. S. Seaman, J. R. Mascola, D. C. Montefiori, Optimization and validation of the TZM-bl assay for standardized assessments of neutralizing antibodies against HIV-1. *J. Immunol. Methods* **409**, 131–146 (2014).doi:10.1016/j.jim.2013.11.022 Medline

46. J. F. Scheid, H. Mouquet, B. Ueberheide, R. Diskin, F. Klein, T. Y. Oliveira, J. Pietzsch, D. Fenyo, A. Abadir, K. Velinzon, A. Hurley, S. Myung, F. Boulad, P. Poignard, D. R. Burton, F. Pereyra, D. D. Ho, B. D. Walker, M. S. Seaman, P. J. Bjorkman, B. T. Chait, M. C. Nussenzweig, Sequence and structural convergence of broad and potent HIV antibodies that mimic CD4 binding. *Science* **333**, 1633–1637 (2011).doi:10.1126/science.1207227 Medline

47. L. M. Walker, S. K. Phogat, P. Y. Chan-Hui, D. Wagner, P. Phung, J. L. Goss, T. Wrin, M. D. Simek, S. Fling, J. L. Mitcham, J. K. Lehrman, F. H. Priddy, O. A. Olsen, S. M. Frey, P. W. Hammond, Protocol G Principal Investigators, S. Kaminsky, T. Zamb, M. Moyle, W. C. Koff, P. Poignard, D. R. Burton, Broad and potent neutralizing antibodies from an African donor reveal a new HIV-1 vaccine target. *Science* **326**, 285–289 (2009).doi:10.1126/science.1178746 Medline

48. L. M. Walker, M. Huber, K. J. Doores, E. Falkowska, R. Pejchal, J. P. Julien, S. K. Wang, A. Ramos, P. Y. Chan-Hui, M. Moyle, J. L. Mitcham, P. W. Hammond, O. A. Olsen, P. Phung, S. Fling, C. H. Wong, S. Phogat, T. Wrin, M. D. Simek, Protocol G Principal Investigators, W. C. Koff, I. A. Wilson, D. R. Burton, P. Poignard, Broad neutralization coverage of HIV by multiple highly potent antibodies. *Nature* **477**, 466–470 (2011).doi:10.1038/nature10373 Medline

49. H. Mouquet, L. Scharf, Z. Euler, Y. Liu, C. Eden, J. F. Scheid, A. Halper-Stromberg, P. N. Gnanapragasam, D. I. Spencer, M. S. Seaman, H. Schuitemaker, T. Feizi,

M. C. Nussenzweig, P. J. Bjorkman, Complex-type N-glycan recognition by potent broadly neutralizing HIV antibodies. *Proc. Natl. Acad. Sci. U.S.A.* **109**, E3268–E3277 (2012).doi:10.1073/pnas.1217207109 Medline

50. M. Thali, J. P. Moore, C. Furman, M. Charles, D. D. Ho, J. Robinson, J. Sodroski, Characterization of conserved human immunodeficiency virus type 1 gp120 neutralization epitopes exposed upon gp120-CD4 binding. *J. Virol.* **67**, 3978–3988 (1993). Medline

51. J. Swetnam, E. Shmelkov, S. Zolla-Pazner, T. Cardozo, Comparative magnitude of cross-strain conservation of HIV variable loop neutralization epitopes. *PLOS ONE* **5**, e15994 (2010).doi:10.1371/journal.pone.0015994 Medline

52. J. Huang, G. Ofek, L. Laub, M. K. Louder, N. A. Doria-Rose, N. S. Longo, H. Imamichi, R. T. Bailer, B. Chakrabarti, S. K. Sharma, S. M. Alam, T. Wang, Y. Yang, B. Zhang, S. A. Migueles, R. Wyatt, B. F. Haynes, P. D. Kwong, J. R. Mascola, M. Connors, Broad and potent neutralization of HIV-1 by a gp41-specific human antibody. *Nature* **491**, 406–412 (2012).doi:10.1038/nature11544 Medline